Annual maps of forest and evergreen forest in the contiguous United States during 2015-2017 from analyses of PALSAR-2 and Landsat images

Jie Wang[1,*], Xiangming Xiao[2,*], Yuanwei Qin[2], Jinwei Dong[3], Geli Zhang[4], Xuebin Yang[2], Xiaocui Wu[5], Chandrashekhar Biradar[6], Yang Hu[7]

[1] College of Grassland Science and Technology, China Agricultural University, Beijing 100093, China
[2] School of Biological Sciences, Center for Earth Observation and Modeling, University of Oklahoma, Norman, OK 73019, USA
[3]Key Laboratory of Land Surface Pattern and Simulation, Institute of Geographic Sciences and Natural Resources Research, Chinese Academy of Sciences, Beijing 100101, China
[4]College of Land Science and Technology, China Agricultural University, Beijing 100193, China
[5]Department of Natural Resources and Environmental Sciences, University of Illinois at Urbana-Champaign, Urbana, IL 61801, USA
[6]Center for International Forestry Research (CIFOR) and World Agroforestry Center (ICRAF), Asia Continental Program, New Delhi, India
[7]School of Ecology and Environment, Ningxia University, Yinchuan 750021, China

Correspondence to: Xiangming Xiao (xiangming.xiao@ou.edu)；Jie Wang (jiewang178@cau.edu.cn)

Abstract: Annual forest maps at a high spatial resolution are necessary for forest management and conservation. Large uncertainties remain among the existing forest maps, because of different forest definitions, satellite datasets, in-situ training datasets, and mapping algorithms. In this study, we generated annual maps of forest and evergreen forest at a 30-m resolution in the Contiguous United States (CONUS) during 2015-2017 by integrating microwave data (Phased Array type L-band Synthetic Aperture Radar (PALSAR-2)) and optical data (Landsat) using knowledge-based algorithms. The resultant PALSAR-2/Landsat-based forest maps (PL-Forest) were compared with five major forest datasets in the CONUS: (1) the Landsat tree canopy cover from Global Forest Watch datasets (GFW-Forest), (2) the Landsat Vegetation Continuous Field datasets (Landsat VCF-Forest), (3) the National Land Cover Database 2016 (NLCD-Forest), (4) the Japan Aerospace Exploration Agency (JAXA) forest maps (JAXA-Forest), and (5) the Forest Inventory and Analysis (FIA) data from the USDA Forest Service (FIA-Forest). The forest structure data (tree canopy height and canopy coverage) derived from the lidar observations of the Geoscience Laser Altimetry System (GLAS) onboard NASA's Ice, Cloud, and land Elevation Satellite (ICESat-1) were used to assess the five forest cover datasets derived from satellite images. Using the forest definition by the Food and Agricultural Organization (FAO) of the United Nations, more forest pixels from the PL-Forest maps meet the FAO's forest definitions than the GFW-, Landsat VCF-, and JAXA-Forest datasets. Forest area estimates from the PL-Forest were close to those from the FIA-Forest statistics but higher than the GFW-Forest, NLCD-Forest and lower than the Landsat VCF-Forest, which highlights the potential of using both PL-Forest and FIA-Forest datasets to support the FAO's Global Forest Resources Assessment. Furthermore, the PL-based annual evergreen forest maps (PL-Evergreen Forest) showed reasonable consistency with the NLCD product. The comparison of the most widely used forest datasets offered insights to employ appropriate products for relevant research and management activities across local to regional and national scales. The generated datasets in this study are available at https://doi.org/10.6084/m9.figshare.21270261(Wang, 2024). The improved annual maps of forest and evergreen forest at 30-m over the CONUS can be used to support forest management, conservation, and resource assessments.

Keywords: Forest map, Evergreen forest map, Tree canopy height, Tree canopy cover

1 Introduction

Forests cover approximately 30% of the land surface and have played major roles in regulating terrestrial carbon and water cycles (Harris et al., 2012; D'almeida et al., 2007), influencing climate (Bonan, 2008; Peng et al., 2014), conserving biodiversity (Seto et al., 2012; Betts et al., 2017), and supplying forest products to humankind (Foley et al., 2005; Smith et al., 2018). The United States of America (USA) is covered by 310 million hectares of forests, which is the fourth largest forest country in the world, as estimated in 2020 (Global Forest Resources Assessment 2020). The forest biomes are dominated by the northwestern rocky mountain and Pacific coast evergreen forests, the eastern deciduous and mixed forests, and the southeastern coastal plain evergreen forests (Cooperation, 1997). The Forest Inventory and Analysis (FIA) program, managed by the U.S. Department of Agriculture (USDA) Forest Service, identified 142 forest types (by major tree species), which were aggregated into 28 forest groups across the USA (Ruefenacht et al., 2008). FIA has reported that the national forest area totals remain stable, but substantial changes occurred at local and regional scales (Oswalt; et al., 2019). In addition, extensive impacts of disturbance (e.g., wildfires, harvests, insect outbreaks) and climate factors have been increasingly changing the forest structure, function, and species composition (Sexton et al., 2016; Mekonnen et al., 2019). It is critical to generate timely and accurate annual forest maps at a high spatial resolution, which can be then used to identify the forest area dynamics， assess the associated impacts，and support policy discussion and relevant research (Sexton et al., 2015).

Remote sensing technology offers large-area and high-frequency observations that have been widely used for regional and global forest mapping. For example, the optical-based regional and global forest maps are generated at the coarse (thousands of meters) and moderate (hundreds of meters) spatial resolutions using the 1-km Advanced Very High Resolution Radiometer (AVHRR) (Hansen and Defries, 2004; Achard et al., 2001), 1-km Satellite Pour I'Observation de Ia Terre 4 (SPOT-4) VEGETATION (Stibig et al., 2004; Stibig and Malingreau, 2003; Souza et al., 2003), and 500-m and 250-m Moderate Resolution Imaging Spectroradiometer (MODIS) (Friedl et al., 2010; Hansen et al., 2003; Dimiceli et al., 2017). The characteristics and comparisons of several major forest cover products at moderate spatial resolution have been shown in detail in one of our previous studies, including image data sources, forest definition, algorithms, accuracy, and other relevant information (Qin et al., 2017).

The Landsat images have been used to generate forest or other land cover products at a high spatial resolution (tens of meters) (Chen et al., 2015; Hansen et al., 2013a; Jin et al., 2013a). The major Landsat-based products for the CONUS include the Global Forest Watch (GFW) program of the World Resources Institute (2013b), the forest cover

fraction (VCF) product from the Global Land Cover Facility Data Center (GLCF) at the University of Maryland (Sexton et al., 2013b), and the National Land Cover Database (NLCD) from U.S. Geological Survey (USGS) (Jin et al., 2013b). In the United States, FIA and NLCD are the primary databases used by managers, researchers, and policymakers to assess land use and track land management (Hoover et al., 2020; Domke et al., 2021). FIA is a field survey of forest plots and reports information on the status and trends of forests in the United States. A subset of plots is measured every year with revisit intervals of 5 to 10 years depending on the state (Hoover et al., 2020; Burrill et al., 2021). The NLCD provides updated datasets every three years or so, which were generated by change detection algorithms for only a time period and had a certain amount of commission errors (Jin et al., 2013a). Additionally, the annual global forest maps have been published by the Japan Aerospace Exploration Agency (JAXA) over the years of 2007-2010 and 2015-2018, which are generated using PALSAR and PALSAR-2 images at 25-m and 50-m spatial resolutions (Shimada et al., 2014). The main characteristics of these high-spatial-resolution forest maps covering the CONUS are summarized in Table 1. The wide availability of satellite-based forest and land cover maps makes it convenient for stakeholders to access more information than ever before. However, it is still challenging for users to understand the differences between the forest products and clarify their application potential for specific purpose systematically.

Due to the differences in forest definitions, satellite data, in-situ training data, and mapping algorithms, the available forest maps still have large discrepancies in forest area estimates (Smith et al., 2018; Qin et al., 2017; Sexton et al., 2016). The optical remote sensing data are affected by cloud cover, cloud shadow, and smoke, which reduce the number of good quality observations (Reiche et al., 2015). Buildings, rocks, and high biomass crops often have large PALSAR backscatter coefficients at similar or higher levels of forest (Qin et al., 2017). The combination of the optical and microwave data could take advantage of the optical remote sensing sensors that capture the light and forest canopy interaction and L-band microwave sensors that capture the microwave and forest structure (tree trunk and branch) interaction without cloud contamination. One study suggested that the complementarity of optical and SAR datasets improved the accuracy of forest maps, in comparison to either optical or SAR dataset (Lehmann et al. 2015). For example, mis-classification of the Landsat-based forest maps could be caused by the re-planted areas with small- or medium-size trees or regions with some vegetation types like highland scrub, however, these regions could be identified correctly by PALSAR data (Lehmann et al. 2015). Improved forest maps have been reported in several studies by using integrated PALSAR and Landsat data in tropical regions (Reiche et al., 2015; Lehmann et al., 2015;

Thapa et al., 2014), and PALSAR and MODIS data in monsoon Asia and other regions of the world (Zhang et al., 2019; Qin et al., 2016b). However, it remains unclear about the potential of combined PALSAR and Landsat images to improve the annual forest area estimates in the CONUS.

In addition to annual forest maps, information on evergreen forests and deciduous forests is also important for forest management and conservation. Many studies showed that the spatial distributions of evergreen and deciduous forests have been changing and will continue to change in the future, driven by multiple stressors involving climate change, forest disturbance, land-use change, and invasive species (Soh et al., 2019; Mekonnen et al., 2019; Knott et al., 2019). Accurate distribution information on evergreen and deciduous forest types is also needed to reduce the uncertainty in the carbon budgets (Deb Burman et al., 2021). With the development of Earth observation technology, some efforts have been carried out to produce forest-type datasets based on multiple spaceborne and/or airborne images (Laurin et al., 2016; Kushwaha, 1990). As an example, for the study at the national or continental scale, the NLCD dataset provides the nationwide distribution of deciduous, evergreen, and mixed forests in the U.S. at 30-m spatial resolution for the years of 2001, 2006, 2011, and 2016. The 50-m evergreen and deciduous forest map in 2010 was generated across monsoon Asia using PALSAR and time series MODIS images (Qin et al., 2016b). In addition, time series MODIS images have been reported to improve the estimates of evergreen forests in tropical regions (Qin et al., 2019). As the NLCD used multi-temporal Landsat images to identify evergreen and deciduous forests, time series Landsat images could improve the discrimination and classification of evergreen and deciduous forests to support the annual analyses in the scientific research and policy-making on forest ecosystems. To date, few efforts have been conducted to produce the annual maps of evergreen or deciduous forests over the temperate regions despite the importance.

The United Nations Food and Agriculture Organization (FAO) Global Forest Resources Assessment (FRA) provides essential information for understanding the world's forest resources, management, and uses every five years since 1990 by assembling the forest data from individual countries (Keenan et al. 2015). In an effort to improve annual forest maps at a national scale to support the FAO FRA program, this study had three objectives. The first objective was to develop annual forest maps and annual evergreen forest maps in the CONUS by using both PALSAR-2 and Landsat images from 2015 to 2017. The second objective was to assess and compare the resultant PALSAR-2/Landsat-based forest maps with the major satellite-based forest cover datasets by using the forest structure data (tree height and tree canopy coverage), which were derived from the observations of the Geoscience Laser Altimetry System

(GLAS) onboard of NASA's Ice, Cloud, and land Elevation Satellite (ICESat-1). This comparison with a large amount of LiDAR data will help understand the differences between the forest datasets under the forest definition used by the FAO. The FAO defines forests as lands of more than 0.5ha with tree cover over 10% and tree height greater than 5-m (Fao, 2012). The third objective was to report the PALSAR-2/Landsat-based forest maps at two administration levels (state and CONUS) and compare them with the forest area estimates from the FIA by the USDA Forest Service, which are the primary data sources provided by the USA government for the FAO Global Forest Resources Assessment. This comparison will help us to investigate the capability of combining the PALSAR-2/Landsat approach and the FIA approach for support of the Global Forest Resource Assessment at the national scale.

Table 1. Characteristics of the main forest cover datasets at a high spatial resolution (tens of meters) for the Contiguous United States. The forest cover datasets analyzed in this study are from the Forest Inventory and Analysis program(FIA-Forest), the National Land Cover Database (NLCD-Forest) from the United States Geological Survey, the Global Forest Watch (GFW-Forest) program of the World Resources Institute, the Landsat-based forest cover fraction (Landsat VCF-Forest) product from the Global Land Cover Facility Data Center at the University of Maryland, the Japan Aerospace Exploration Agency forest maps (JAXA-Forest), and the PALSAR-2/Landsat-based forest maps generated in this study (PL-Forest).

Sensors	Datasets	Forest definition	Major data source	Methods	Spatial resolutions	Periods	References
Statistics	FIA-Forest	Tree cover≥10%	Inventory data	Sampling	State	Annual sampling design after 1998	Burrill et al. (2021)
Optical	NLCD-Forest	Tree cover≥ 20%, tree height ≥ 5-m	Landsat images	Decision tree	30-m	circa 1992, 2001, 2006, 2011, 2016, 2019	Jin et al. (2019)
	Landsat VCF-Forest	tree height ≥ 5-m	MODIS VCF, Landsat images	Regression tree	30-m	2000, 2005, 2010, 2015	Sexton et al. (2013a)
	GFW-Forest	tree height ≥ 5-m	Landsat images	Decision tree	30-m	2000, 2010	Hansen et al. (2013a)
SAR	JAXA-Forest	Tree cover ≥ 10%, tree height ≥ 5-m	PALSAR/PALSAR-2 images	Decision tree	25-m	2007-2010, 2015-2018	Shimada et al. (2014)
SAR/Optical	PL-Forest	Tree cover ≥ 10%, tree height ≥ 5-m	25-m PALSAR-2 and 30-m Landsat images in 2015-2017	Decision tree	30-m	2015-2017	This study

2 Materials and Methods

The workflow in Fig. 1 presents the three major study sections and the detailed processes of each section in this study. First, we generated the annual forest maps, and annual evergreen and deciduous forest maps at 30-m spatial resolution during 2015-2017 by integrating PALSAR-2 and Landsat time-series Normalized Difference Vegetation Index (NDVI) data. Second, we compared the resultant PALSAR-2/Landsat forest maps with other major satellite-based forest datasets in the study period of 2015-2017. We assessed these forest maps following the FAO's forest definition using the tree height and canopy coverage data from the ICESat-1 LiDAR-based products. Third, we examined the performance of all the satellite-based forest maps on forest area estimates by comparison with the FIA statistic data at the state and national administration levels.

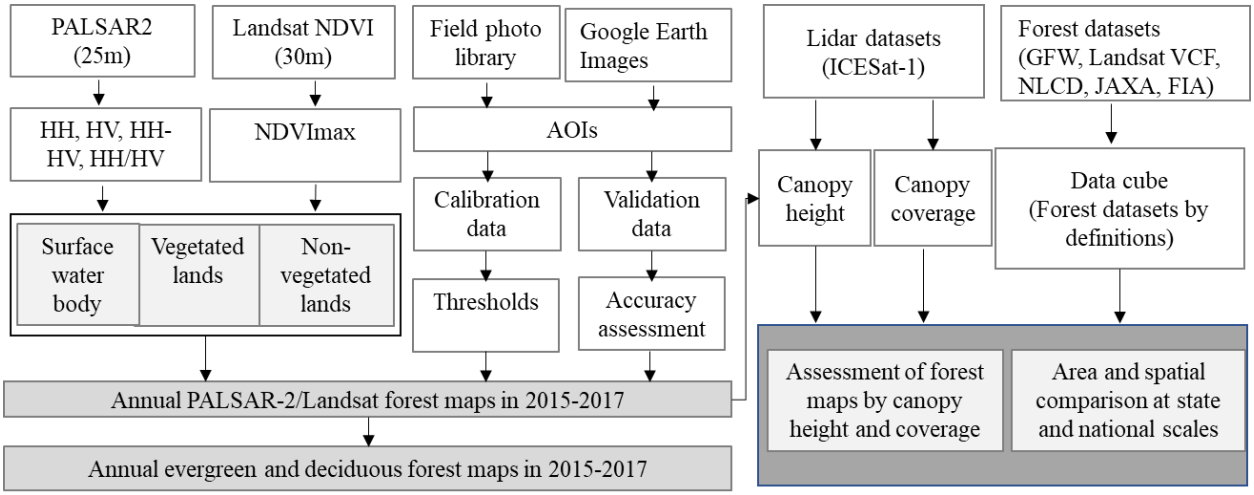

Figure 1: The workflow of this study. It includes three major study sections and the detailed processes of each section in this study. GFW, Landsat VCF, NLCD, JAXA, and FIA present different forest cover datasets that have been released. HH, HV, HH-HV, and HH/HV denote the horizontal-horizontal (HH) and horizontal-vertical (HV) polarization bands, and two composite layers of the difference (HH-HV) and the ratio (HH/HV). AOIs refer to the areas of interest used as calibration and validation samples in this study.

2.1 Study area

Our study area is the CONUS with an area of about 8.08×10^6 km^2, including the 48 states and Washington, DC. About 50% of the CONUS land cover change has involved forests since 2001(Homer et al., 2020). The CONUS has large topographical variation from the eastern USA to the western USA as shown by the spatial distribution of topography in the CONUS (Fig. 2a).

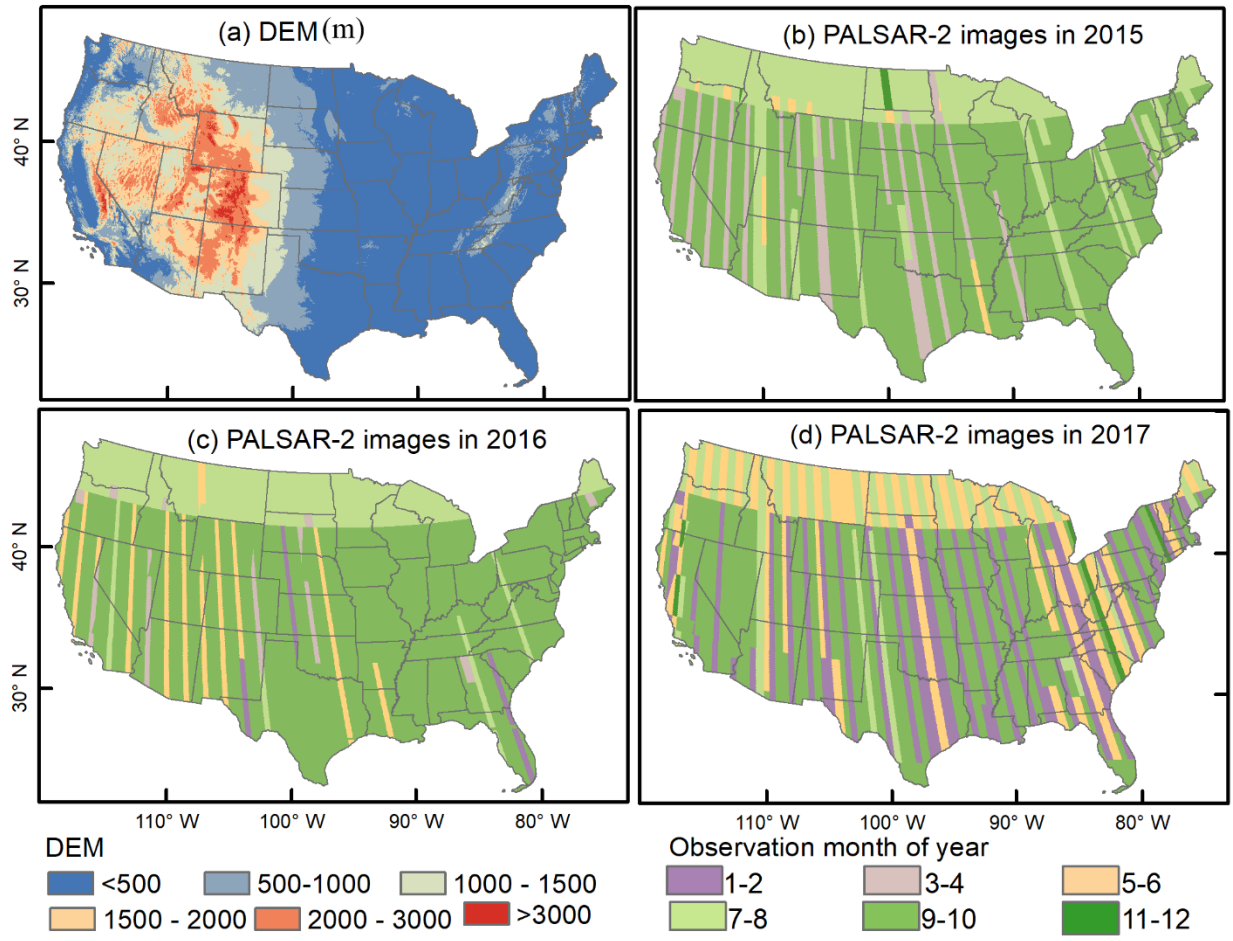

Figure 2: The spatial distributions of (a) the topography of the CONUS using the data from the U.S. Geological Survey, 3D Elevation Program 10-Meter Resolution Digital Elevation Model (DEM). (b, c, d) the acquisition dates of PALSAR-2 images in a year during2015 - 2017.

2.2 PALSAR-2 data in 2015-2017

The annual 25-m ALOS-2 PALSAR-2 mosaic data from 2015 to 2017 were collected at the Google Earth Engine (GEE) platform (https://developers.google.com/earth-engine/datasets/catalog/JAXA_ALOS_PALSAR_YEARLY_SAR, last access: 18 March 2022). The PALSAR-2 horizontal-horizontal (HH) and horizontal-vertical (HV) polarization bands, provided by the Earth Observation Research Center, Japan Aerospace Exploration Agency (JAXA), are slope-corrected, radiometrically calibrated, and ortho-rectified backscatters with a geometric accuracy of around 12 meters (Reiche et al., 2018). Fig. 2b,c,d shows the acquisition dates of the PALSAR-2 mosaic images over the CONUS and most images were acquired from May to October. The HH and HV bands were converted from the amplitude values into gamma-naught backscattering coefficients in decibels (γ^0) using the equation (1) (Shimada et al., 2009; Shimada et al., 2014; Chen et al., 2018).

$$\gamma^{\circ}=10\times ln\mathrm{DN}^2 + \mathrm{CF} \quad (1)$$

where γ° is the backscattering coefficient using dB as the unit; DN is the digital number of the amplitude images like HH or HV band, and CF is a calibration factor with a value of -83 dB. In addition, two composite layers, i.e., the difference (HH-HV) and the ratio (HH/HV), were calculated as input data for forest mapping.

2.3 Landsat data in 2015-2017

We used all the Landsat-7 Enhanced Thematic Mapper (ETM+) and Landsat-8 Operational Land Imager (OLI) surface reflectance (SR) images from 2015 to 2017 to construct a time series image data cube in GEE (https://developers.google.com/earth-engine/datasets/catalog/LANDSAT, last access: 18 March 2022). This dataset provides multi-spectral images at 30-m resolution and the SR data were derived from top-of-atmosphere (TOA) reflectance by the atmospheric correction codes (Vermote et al., 2016). The bad-quality observations with clouds, cloud shadows, snow/ice, and scan-line-off strips were identified as NODATA following the quality band (pixel_qa). The remaining good-quality observations were used to calculate the vegetation indices of NDVI, Enhanced Vegetation Index (EVI), and Land Surface Water Index (LSWI) for each image in the data cube. Fig. 3 shows the spatial distribution of annual total good-quality observation numbers (GOBs) for individual pixels over the CONUS from 2015 to 2017.

$$NDVI = \frac{\rho_{NIR}-\rho_{Red}}{\rho_{NIR}+\rho_{Red}} \quad (2)$$

$$EVI = 2.5 \times \frac{\rho_{NIR}-\rho_{Red}}{\rho_{NIR}+6\times\rho_{Red}-7.5\times\rho_{Blue}+1} \quad (3)$$

$$LSWI = \frac{\rho_{NIR}-\rho_{SWIR}}{\rho_{NIR}+\rho_{SWIR}} \quad (4)$$

where $\rho_{Blue,}$ ρ_{Red} ρ_{NIR} and ρ_{SWIR} are the surface reflectance values of blue (450-520nm), red (630-690nm), near-infrared (760-900nm), and shortwave-infrared bands (1550-1750nm).

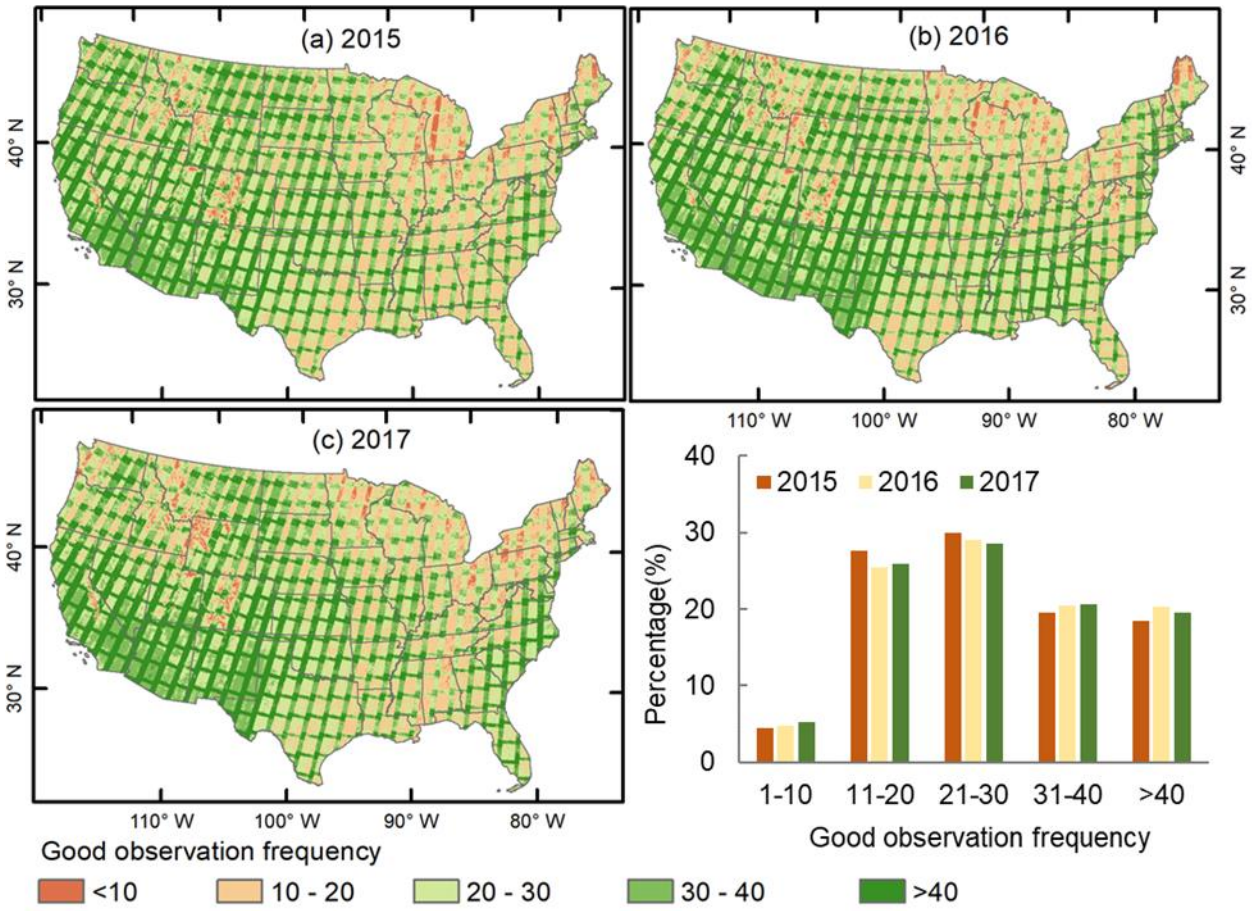

Figure 3: The summary of the good-quality observation (GOBs) numbers for individual pixels in a year over the CONUS using all Landsat images in a year from 2015 to 2017.

2.4 Sample data for accuracy assessment of forest maps

The accuracy of the PALSAR-2/Landsat annual forest maps was assessed based on the global validation sample set released by researchers from Tsinghua University, China (http://data.ess.tsinghua.edu.cn/, last access: 20 February 2022) (Gong et al., 2013). This validation dataset was generated using a random sampling strategy and visual interpretation method for the Finer Resolution Observation and Monitoring-Global Land Cover (FROM-GLC) (Gong et al., 2013). As the validation samples were generated in 2013, in this study, we double-checked the land cover types of all the samples by visual interpretation of the Google Earth images during 2015-2017. We deleted those samples with land cover changes (e.g., from forest to non-forest or from non-forest to forest), and thus, a total of 652 forest samples were kept for this study. At last, a total number of 1,958 points were used for the validation of the resultant forest maps, which include 652 forests, 285 croplands, 431 grasslands, 205 shrublands, 95 water bodies and wetlands, 46 impervious surfaces, 244 barren lands (Fig. 4).

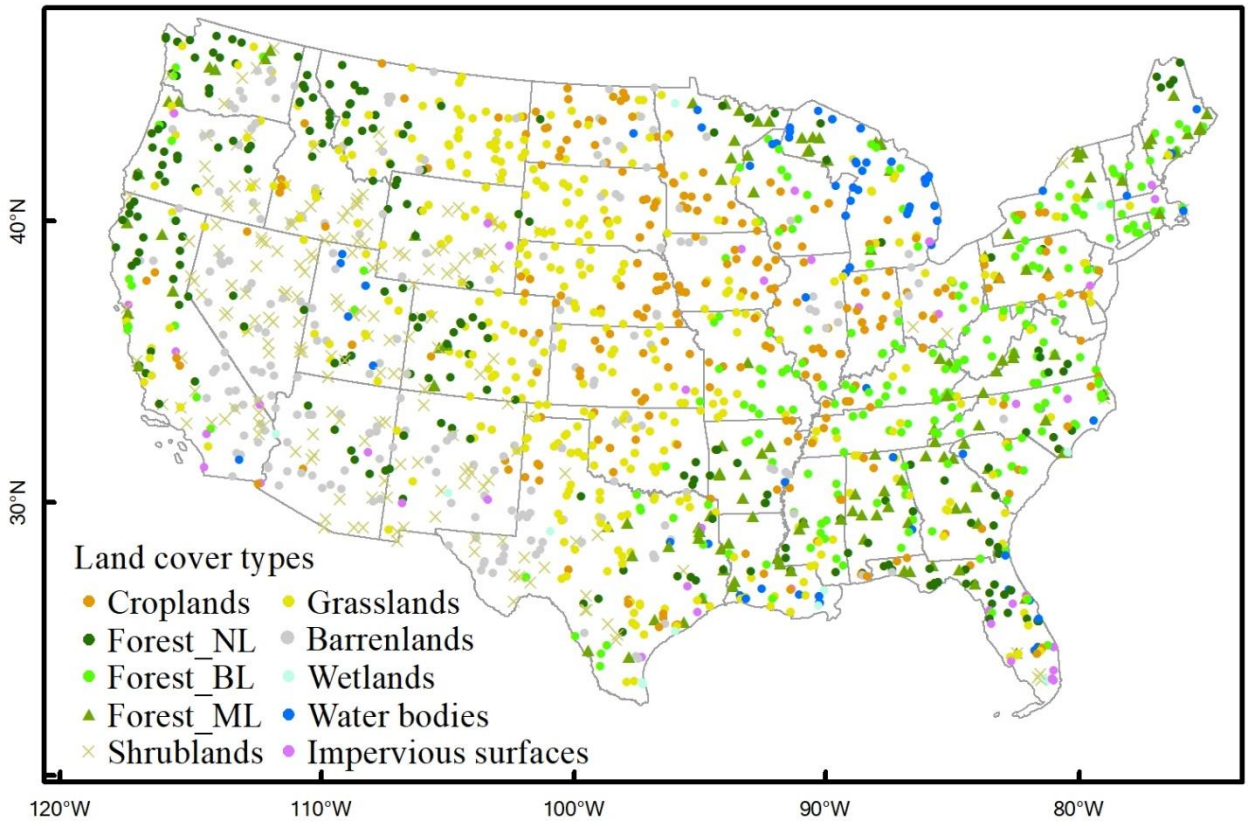

Figure 4: The land cover samples for accuracy assessment in this study. These samples were from the global validation sample set released by the researchers from Tsinghua University, China (http://data.ess.tsinghua.edu.cn/, last access: 20 February 2022) (Gong et al. 2013). They were revised by excluding the samples with land cover change according to the Google Earth images. Forest_NL, Forest_BL, and Forest_ML denote needle-leaved forest, broad-leaved forest, and mixed-leaved forest, respectively.

2.5 Canopy height and canopy coverage data from ICESat LiDAR

To assess the PALSAR-2/Landsat forest maps and other forest maps in terms of forest structure traits (canopy height, canopy coverage) that are used in forest definition by FAO, we used the ICESat global canopy coverage and height dataset to generate the samples of (1) forest canopy height (meter) and (2) forest canopy coverage (%). This ICESat dataset was derived based on the observations from the Geoscience Laser Altimetry System (GLAS) on board NASA's Ice, Cloud, and land Elevation Satellite (ICESat-1) with a footprint of about 65-m in diameter (Tang et al., 2019). The ICESat mission acquired LiDAR data over the globe during 2003-2009. The ICESat-based tree canopy cover products provide improved information to characterize biome-level gradients and canopy cover almost without bias at the footprint level (Tang et al., 2019). There are more than 550,000 laser footprints from ICESat-1 over the CONUS (Fig. 5). This is the only available dataset that can be used to assess the structural characteristics of the forests

extracted by the forest cover products in the study period of 2015-2017. The image acquisition years differ between the ICESat data (2003-2009) and the PALSAR-2/Landsat data (2015-2017), which may cause small uncertainties in the assessment results. A pixel has three scenarios in terms of forest or not in these two time periods (2003-2009 vs 2015-2017): (1) as forest in both 2003-2009 and 2015-2017, (2) as forest in 2003-2009 but not in 2015-2017 (forest loss due to deforestation), and (3) as forest in 2015-2017 but not in 2003-2009 (forest gain due reforestation or afforestation). For those pixels that were forest in both 2003-2009 and 2015-2017 (Scenario #1), as the canopy height (CH) and canopy coverage (CC) of a forest stand are likely to increase over the years, using CH and CC data in 2003-2009 may underestimate the number of pixels meets the FAO forest definition. For those pixels that were forest only in one period of 2003-2009 or 2015-2017 (scenario #2 or #3), they were not evaluated in the assessment. In addition, the differences in image acquisition years would not affect the results of inter-comparison between different forest cover products.

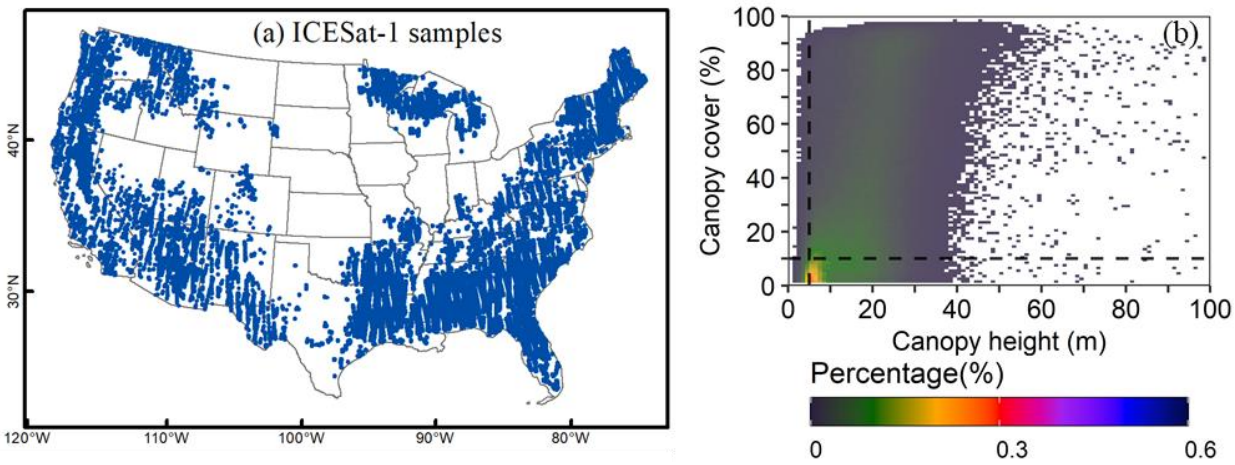

Figure 5. The ICESat samples in the CONUS, (a) Spatial distribution of ICESat-1 samples. (b) the histogram of canopy height (m) and canopy coverage (%) for the ICESat-1 samples.

2.6 Satellite-based forest cover data products for inter-comparison

We used four forest cover products derived from analyses of satellite images at a high spatial resolution (≤30-m) for inter-comparison with our PALSAR-2/Landsat forest maps: the GFW product in 2010, the Landsat VCF product in 2015, the NLCD product in 2016 (NLCD2016), and JAXA product in 2015-2017 (Fig. 6). The GFW tree canopy cover product in 2010 at 30-m resolution was generated by using decision tree algorithms and multi-temporal Landsat images (https://www.glad.umd.edu/dataset/global-2010-tree-cover-30-m, last access: 1 May 2021) (Hansen et al., 2013a). The Landsat VCF product in 2015 is a global tree cover percentage dataset and can be downloaded from the Land-Cover and Land-Use Change Program (https://lcluc.umd.edu/metadata/global-30m-landsat-tree-canopy-

version-4, last access: 5 May 2021). It is generated by using a regression tree model to rescale the 250-m MODIS VCF tree cover layer into 30-m (Sexton et al., 2013a). The Landsat-based NLCD2016 provides land cover information at 30-m resolution over the CONUS with an accuracy of 83% (https://www.mrlc.gov/data/nlcd-2016-land-cover-conus, last access: 9 May 2021) (Homer et al., 2020). This product has three forest types: deciduous forest, evergreen forest, and mixed forest (Homer et al., 2020). The 25-m annual global forest maps from 2015 to 2017 from JAXA were produced by using thePALSAR-2 mosaic data and a decision tree method (JAXA-Forest maps), which are available at https://www.eorc.jaxa.jp/ALOS/en/palsar_fnf/fnf_index.html, with last access of 12 May 2021 (Shimada et al., 2014). JAXA-Forest used the FAO forest definition. So, similarly, for the tree cover products of Landsat VCF and GFW, we selected the pixels with tree canopy coverage greater than 10% as forests to generate the GFW-Forest and Landsat VCF-Forest maps.

2.7. Forest cover data from in-situ field inventory for inter-comparison

The forest area statistical data for year 2017 at the county scale was also used for comparison analysis. This statistical dataset comes from the USDA Forest Service (FS) FIA program (https://www.srs.fs.usda.gov/pubs/57903, last access: 10 May 2021) and is widely used in the studies of forests in the CONUS (Domke et al., 2021; Burrill et al., 2021; Hoover et al., 2020). The definition of the forest land condition is: larger than 0.4 ha (1.0 acre) in size, greater than 37m (120.0 feet) in width, at least 10% canopy cover by live tally trees of any size at present or in the past (Burrill et al., 2021). Forest land also includes (1) the transition zones, such as areas between forest and non-forest lands that meet the minimal tree canopy cover and forest areas; (2) the strips of trees in roadside, streamside, and shelterbelt, must wider than 37m (120 feet) and longer than 111m (363 feet) continuously; (3) the unimproved roads and trails, streams, and clearings in forest areas if they are less than 37m in width or less than 0.4 ha in size. Forest land does not include tree-covered regions in agricultural production settings like orchards or urban areas like city parks (Burrill et al., 2021). The accuracy standard for forest area in the FIA program is to meet the mandated sampling error no more than 3% error per 1 million acres of timberland (Burrill et al., 2021). It is the critical data source provided by the US government for the FAO's Global Forest Resources Assessment, and for resources managers and the public to manage and utilize the forest resources in the United States.

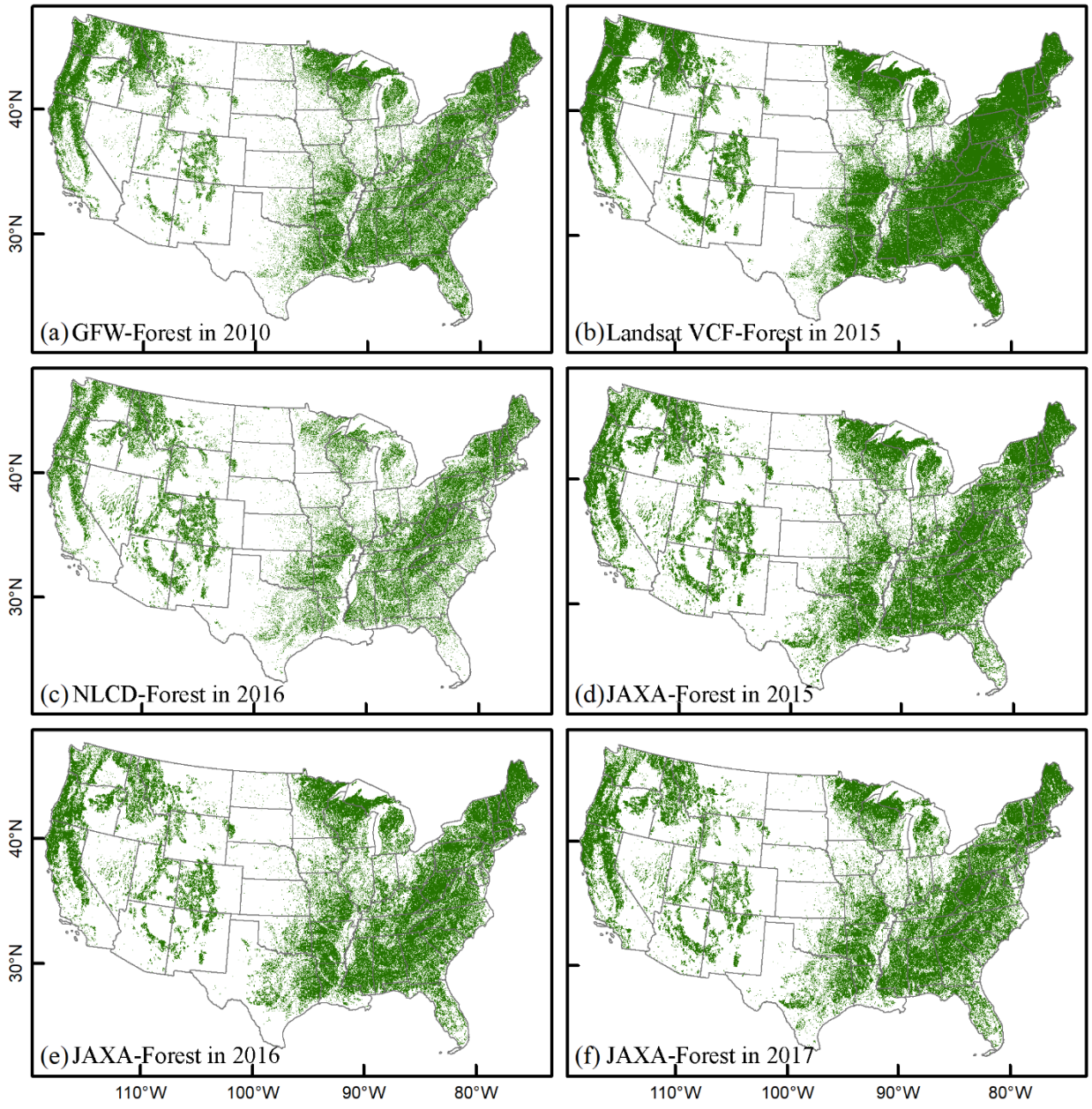

Figure 6. Forest distribution in the CONUS from four forest data products, (a, b, c) Landsat-based and (d, e, f) PALSAR-2-based forest products during 2015-2017. GFW-Forest in 2010 presents the forest cover map in 2010 from the Global Forest Watch (GFW) program of the World Resources Institute. Landsat VCF-Forest in 2015 presents the Landsat-based forest cover fraction (Landsat VCF) product from the Global Land Cover Facility Data Center at the University of Maryland. NLCD-Forest in 2016 presents the forest cover map in 2016 from the National Land Cover Database (NLCD). JAXA-Forest in 2015-2017 refer to the Japan Aerospace Exploration Agency forest maps from 2015 to 2017.

2.8 PALSAR-2/Landsat forest mapping approach

The advantages of L-band ALSO-2 PALSAR-2 data in penetrating tree canopy to interact with tree branches and trunks lead to higher volume backscatter signals from forests than from other land cover types (e.g., grasslands,

shrublands, croplands, and water bodies). However, some natural surfaces (e.g., rocky lands) or artificial structures (e.g., buildings) also have high backscatter signals, which could easily cause commission errors in the PALSAR/PALSAR-2-based forest signature analysis (Qin et al., 2017). As these land cover types have low NDVI values, they can be tracked and identified by optical images. According to this knowledge, we developed a two-step forest mapping approach by integration of PALSAR or PALSAR-2 and optical (e.g. MODIS, Landsat) images in our previous studies such as in South America (Qin et al., 2017), Asia (Qin et al., 2016b), and Australia (Qin et al., 2021). However, these previous studies were mainly conducted at a lower spatial resolution (e.g., 50-m by PALSAR and MODIS) or attempted for limited spatial scales using PALSAR/PALSAR-2 and Landsat images. It is still unclear the performance of the integrated datasets of PALSAR-2 and Landsat for monitoring annual dynamics of forest distribution and forest functional types over the temperate regions at a higher spatial resolution of 30-m.

In this study, we used the same workflow (Qin et al., 2016a) to identify and map forest cover in CONUS. First, we identified forest pixels by using 25-m PALSAR-2 images and the threshold-based algorithm. A pixel is classified to be pixel forest, if its PALSAR-2 data meets $-19 \leq HV \leq -7.5$, $0 \leq Difference \leq 9.5$, $0.2 \leq Ratio \leq 0.95$. The thresholds for the 25-m PALSAR-2 images had been slightly adjusted from those for the 25-m PALSAR data based on our previous studies on PALSAR and PALSAR-2 signature analyses of forest and non-forest samples (Qin et al., 2016a; Chen et al., 2018). A 5×5 window median filter was applied to decrease the potential noise (e.g., salt-and-pepper noise) on the PALSAR-based forest and non-forest (F/NF) maps. These resultant 25-m F/NF maps were resampled to 30-m to match the spatial resolution of Landsat images. Forests usually have a high leaf area index (larger than 3 m^2/m^2), but rocky lands, barren lands, and built-up surfaces have no or little green vegetation in a year. Due to LAI and NDVI are closely related to each other, the value of NDVI with 0.7 or so usually represents the range of 1 to 2 m^2/m^2 of LAI dependent upon the vegetation types, which can be used to identify forest and eliminate the commission errors in the PALSAR/PALSAR-2 based forest maps (Qin et al., 2016a). Here we generated the maximum NDVI layers from all the available Landsat images in each year (January to December) during 2015-2017 and applied the threshold of $NDVI_{max} > 0.7$ into the layers to generate the NDVImax masks to extract the pixels covered by green vegetation. The annual 30-m forest map was produced by overlaying the PALSAR-2-based forest maps and the Landsat-based NDVImax mask layers.

In post-classification, a temporal and logical consistency check was performed on this three-year forest and non-forest (F/NF) maps to reduce the noise or misclassification in the F/NF sequence (Chen et al., 2018; Qin et al., 2016a).

For each pixel in annual F/NF time series maps from 2015 to 2017, the reasonable forest dynamics were NNN, FNN, NNF, FFF, NFF, and FFN (N denotes non-forest and F indicates forest). The NFN and FNF sequences were considered as "not reasonable sequences" and re-processed as sequences of NNN and FFF, respectively. This 3-year consistency check during 2015-2017 makes the annual forest map in 2016 with higher confidence, and we will use it for inter-comparison and forest area estimates at county, state, and CONUS scales. The resultant PALSAR-2/Landsat (PL-) annual forest maps are called "PL-Forest maps" in this study.

2.9 PALSAR-2/Landsat-based annual evergreen forest maps in 2015-2017

Evergreen trees have green leaves all year round, but deciduous trees usually shed their leaves in winter or dry season. These leaf phenological profiles can be captured by the satellite-based vegetation indices (e.g., NDVI, EVI, and LSWI) to distinguish evergreen and deciduous forests (Qin et al., 2016b; Prabakaran et al., 2013). Based on the characteristics of forest canopy phenology and vegetation indices, we have developed a simple and robust algorithm to map evergreen forests by analyzing the time series water-related index (LSWI) and greenness-related indices (EVI, NDVI). The green leaves of evergreen forests have positive LSWI values all year round and relatively high EVI in winter and/or dry seasons, and thus the seasonal profiles analysis of LSWI and EVI was used to identify evergreen forests (Qin et al., 2016b). The same approach was used to generate the annual maps of evergreen vegetation by the criteria of pixels having (1) LSWI≥0 for all the good observation images in a year and (2) a minimum EVI (EVI_{min}) no less than 0.2 identified as evergreen cover. This rule can be characterized by the frequency of LSWI≥0 ($FQ_{LSWI\geq0}$) for all the good observations in a year and EVI_{min} using the decision thresholds ($FQ_{LSWI\geq0}$ = 100% and $EVI_{min} \geq 0.2$). Here, the $FQ_{LSWI\geq0}$ was calculated by the number of observations with LSWI≥0 ($N_{LSWI\geq0}$) over the number of good-quality observations (N_{GOBs}) in a year for individual pixels (EQ. 4). Finally, we overlaid our annual 30-m PALSAR-2/Landsat-based forest/non-forest map with the evergreen vegetation layer to identify evergreen forests. Thus, evergreen forests refer to the forest land having green leaves throughout the year, with tree canopy height greater than 5-m and tree canopy cover larger than 10%. In this study, both the forests and evergreen forests include natural and artificial forests that meet the requirements (Qin et al., 2024). Meanwhile, as the evergreen forests were extracted based on the greenness signature observed by the satellite images, this map includes both needle-leaf and broad-leaf evergreen forests that meet the requirements.

$$FQ_{LSWI\geq0} = \frac{N_{LSWI\geq0}}{N_{GOBs}} \times 100 \quad (4)$$

2.10 Validation

The resultant PL-Forest maps (forest and non-forest) in 2015-2017 were validated by the validation samples generated by the researchers from Tsinghua University, China (Gong et al., 2013) (Fig.4). We overlayed the samples and the resultant PL-Forest maps to calculate the confusion matrix and assess the user's, producer's, and overall accuracies.

2.11 Cross-comparison between forest-related products

We selected the five forest cover data products at 25-m or 30-m spatial resolution to perform the inter-comparison analysis at three spatial scales: (1) forest/non-forest with forest height and canopy coverage data at pixel scale, (2) forest area estimates at state scale, and (3) forest area estimates at the CONUS scale.

First, to understand the differences in terms of forest structure measurements in the PALSAR-2-based, Landsat-based, and PALSAR-2/Landsat-based forest maps, we overlaid the ICESat-1 samples and individual forest products to identify those forest pixels that geographically correspond to the ICESat-1 samples and gather their information on the attributes of forest canopy height and canopy coverage. In this process, all the forest products have been resampled into 70-m to match the footprint size of ICESat-1. Then, the distributions of forest pixels were analyzed with the canopy height and canopy coverage for individual forest maps by using 1-D histogram and 2-D histogram graphs.

Secondly, we compared our PL-based forest maps with the selected five forest datasets in terms of forest areas at state scale. All the forest maps were re-projected into equal-area projection before the forest areas were calculated from individual maps. The linear regression approach was used to show the relationships in forest areas between these forest datasets at the state level.

Thirdly, the forest area estimates at the national level were directly compared among them. Based on the re-projected forest maps, the forest areas were calculated at the CONUS region from each individual maps. The results on the forest area of CONUS were compared among them.

3 Results

3.1 Annual forest and evergreen forest maps in 2015-2017

The PALSAR-2/Landsat forest maps show the annual forest distribution in CONUS from 2015 to 2017 (Fig.7a, b, c). At the pixel level, we calculated the frequency of individual pixels covered by forest in 2015-2017 (Fig.7d). 79% of the forest pixels have consistent forest cover from 2015 to 2017 with a frequency of three, which is much larger

than the proportions of forest pixels with one year (11%) or two years (10%) forest cover. The forest dynamics from 2015 to 2017 are shown in Fig.7e, f. It suggested that more forest decreases than forest increases, especially for the central regions.

Based on the validation samples (Fig.4), the accuracies of the PALSAR-2/Landsat forests were high and varied slightly for the years of 2015 to 2017, the overall accuracies of ~93%, the user's accuracies of 87.6% to 95.8%, and producer's accuracies of 90.6% to 91.9% (Table 2). The forest map in 2016 had slightly higher accuracy than in 2015 and 2017, which was expected because the temporal and logical consistency check was implemented on the resultant map of 2016 to reduce the noise or misclassification in the F/NF sequence of 2015 to 2017 (see Section 2.7). The accuracies were comparable to the PALSAR-based forest maps that reported overall accuracies exceeding 91% (Shimada et al., 2014). In detail, the accuracies of the PALSAR-2/Landsat forests in 2016 have been estimated at different altitudes of 0-500m, 500-1000m, 1000-2000m, and 2000-4000m (Tabel 3). Results showed that the areas with altitudes lower than 2000m have user's and producer's accuracies greater than 88%, and overall accuracies greater than 91%. The areas with altitudes higher than 2000m have slightly lower user's (78.3%), producer's (76.6%), and overall accuracies (87.8%). Additionally, we examined the potential of the PALSAR-2/Landsat forests in 2016 to exclude the impacts of the burned area by overlying a MODIS burned area product and the forest map (Fig. 8). The results showed that there were 6,845,692 pixels covered by burned area and 713,003 pixels were identified as forests in the resultant PALSAR-2/Landsat forest map in 2016 with a proportion of about 10.4%. But this number may not

accurately represent the commission error, as the burned forest may not be fully dead and could regrow again.

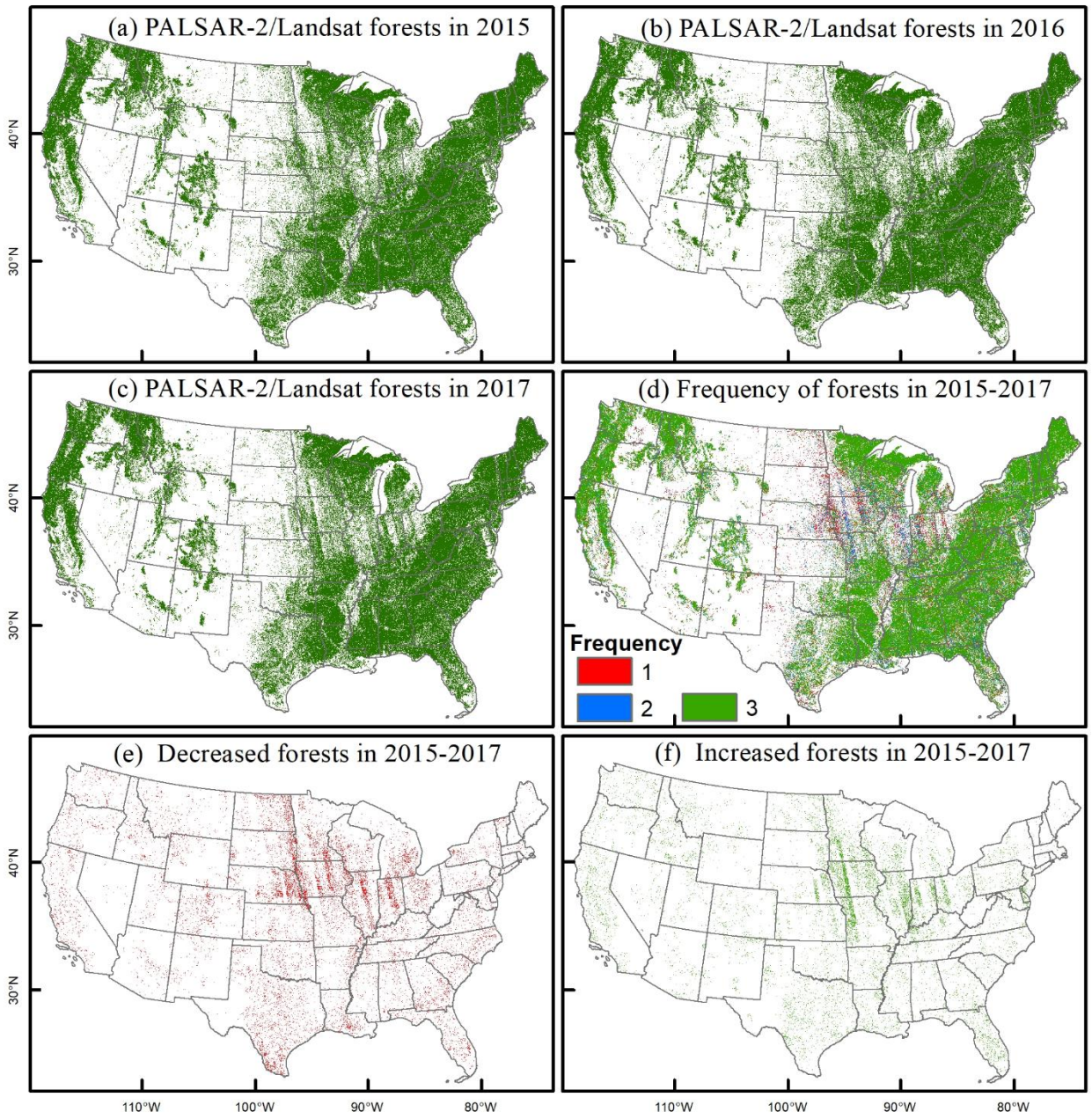

Figure 7: Annual forest maps in 2015-2017 based on PALSAR-2 and Landsat images (PL-Forest), (a) PL-Forest in 2015, (b) PL-Forest in 2016, and (c) PL-Forest in 2017. (d) the forest frequency map was generated based on the PL-Forest maps in 2015-2017. The colors red, blue, and green denote the numbers of a specific pixel classified as forest in the annual PL-Forest maps from 2015 to 2017. (e) the decreased forest in 2015-2017. (f) the increased forest in 2015-2017.

Table 2. Accuracy assessment of annual PALSAR-2/Landsat forest maps in 2015-2017 (PL-Forests) based on the validation samples (Fig.4). The User's (UA), Producer's (PA), and Overall (OA) accuracy are shown.

PL-Forests Classification		Reference			UA	PA	OA
		Forests	Non-Forests	Total			
2015	Forests	596	84	680	87.6%	91.4%	92.8%
	Non-forests	56	1222	1278	95.6%	93.5%	
	Total	652	1306	1958			
2016	Forests	599	81	680	88.1%	91.9%	93.2%
	Non-forests	53	1225	1278	95.8%	93.8%	
	Total	652	1306	1958			
2017	Forests	591	84	675	87.6%	90.6%	92.6%
	Non-forests	61	1222	1283	95.2%	93.5%	
	Total	652	1306	1958			

Table 3. Accuracy assessment of the annual PALSAR-2/Landsat forest map in 2016 (PL-Forests) with different elevations based on the validation samples (Fig. 4). The User's (UA), Producer's (PA), and Overall (OA) accuracy is shown.

Elevation (m)	PL-Forests Classification	Reference			UA	PA	OA
		Forests	Non-Forests	Total			
0-500	Forests	441	58	499	88.4%	94.0%	91.2%
	Non-forests	28	555	583	95.2%	90.5%	
	Total	469	613	1092			
500-1000	Forests	70	6	76	92.1%	90.9%	95.9%
	Non-forests	7	234	241	97.1%	97.5%	
	Total	77	240	317			
1000-2000	Forests	52	7	59	88.1%	88.1%	96.4%
	Non-forests	7	321	328	97.9%	97.9%	
	Total	59	328	387			
2000-4000	Forests	36	10	46	78.3%	76.6%	87.8%
	Non-forests	11	115	126	91.3%	92.0%	
	Total	47	125	172			

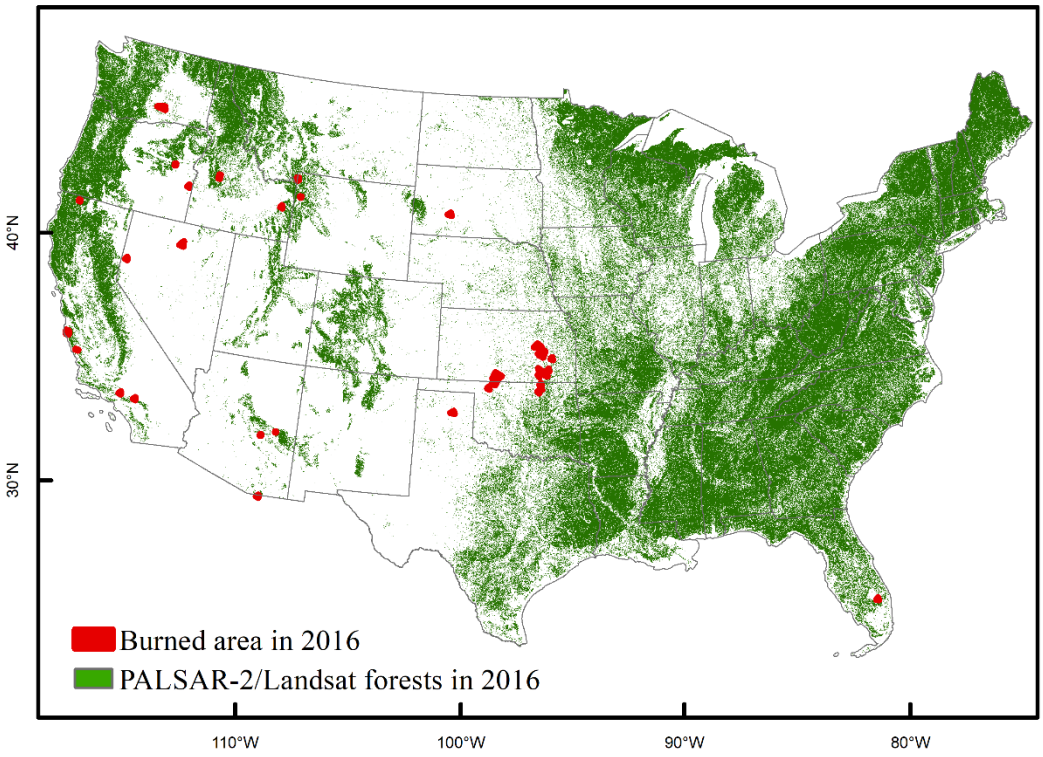

Figure 8: Distribution of burned area overlaid with the PALSAR-2/Landsat forests in 2016. The burned area in 2016 was generated from the MODIS Burned Area Monthly Global 500m products (MCD64A1.061). If a pixel was burned in any month, the pixel was considered a burned area in 2016.

Based on the PALSAR-2/Landsat forest maps, we further identified annual evergreen forests in CONUS during 2015-2017 (Fig. 9a, b, c). These resultant evergreen forest maps have similar spatial patterns with the evergreen forests in the NLCD-2016 dataset (Fig. 9d). Evergreen forests show obvious regional characteristics and are mainly distributed in the western, southeastern, and northeastern regions of the CONUS. The evergreen forest area estimated from the PALSAR-2/Landsat map in 2016 was 1.08×10^6 km^2, which is higher than the evergreen forests of 0.92×10^6 km^2 but lower than the total area of evergreen forests and mixed forests of 1.22×10^6 km^2 from the NLCD-2016 (Fig. 9a-d). The spatial comparison between these two products was carried out at the pixel scale (Fig. 9e). The noticeable discrepancies were in the southwestern regions (e.g., Nevada, Utah, Arizona), south Florida, and some regions in the northeastern CONUS. In the southwestern regions, the differences were mainly from the detection of evergreen and non-evergreen forests between these two products. For the eastern regions (e.g., south Florida, and New England states), the differences between these two products were mostly caused by the detection of forests, as most of the evergreen forest pixels in the PALSAR-2/Landsat evergreen forest map were shown as non-forest in the NLCD map (Fig. 9e). At the state scale, the PALSAR-2/Landsat evergreen forest map in 2016 had a good linear relationship with

the evergreen forests in NLCD 2016, with a slope of 0.8 and R^2 of 0.54 (Fig. 9f). A stronger relationship was found between the evergreen forest areas from the PL-Evergreen forest maps and the sum of evergreen forest and mixed forests from the NLCD-2016 at the state scale, with a slope of 0.98 and R^2 of 0.69 (Fig. 9f). One possible explanation could be that the mixed forests in NLCD include evergreen species (Selkowitz and Stehman, 2011). However, it cannot be estimated quantitatively because it is uncertain about the forest types and proportions within the mixed forest pixels (Tran et al., 2016).

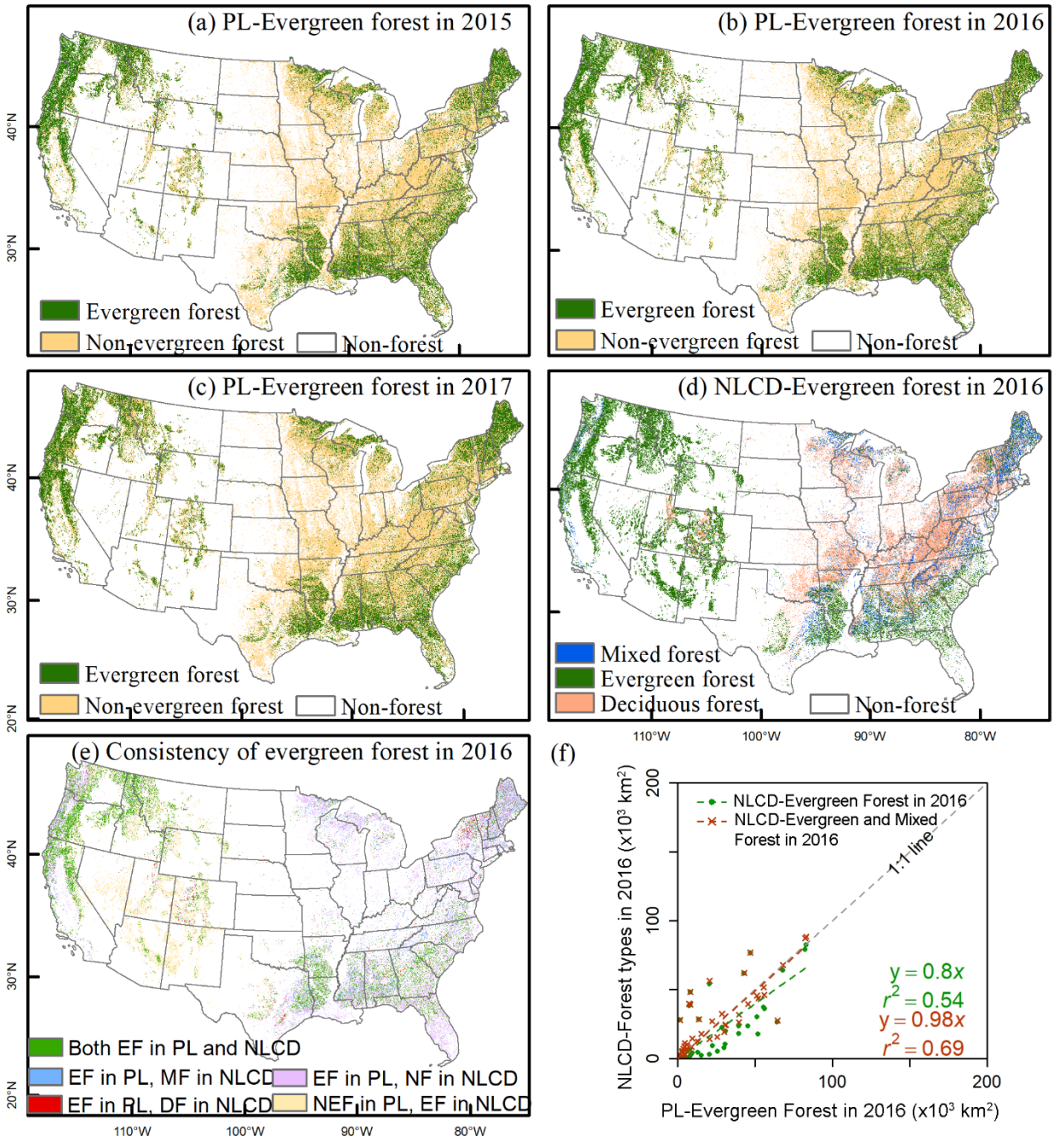

Figure 9: Spatial distributions of evergreen forests in the CONUS. (a, b, c) Annual evergreen and non-evergreen forest maps generated from the PALSAR-2/Landsat (PL) images in 2015-2017. (d) The forest-type map from the National Land Cover Database (NLCD) in the 2016 dataset. (e) shows the consistency between the PL-Evergreen forest in 2016 and the NLCD-Evergreen forest in 2016. The abbreviations are Evergreen Forest (EF), PL-Evergreen Forest in 2016 (PL), Mixed Forest (MF), Non-Forest (NF), Deciduous Forest (DF), and Non-Evergreen Forest (NEF). (f) shows the comparison between PL-Evergreen forest and NLCD-Evergreen and NLCD-Evergreen and mixed forest in 2016 at the state scale using the linear regression analysis.

3.2 A comparison of five satellite-based forest maps at the pixel scale

At the pixel scale, we compared the PALSAR-2/Landsat forest and the JAXA-Forest in 2016 in terms of forest area identification (Fig. 10). These two products have about 75% pixels in agreement, 11% pixels only identified by the JAXA-Forest, and 14% pixels only identified by the PALSAR-2/Landsat forest product. Comparison through zoom-in random samples showed that some pixels with obvious backgrounds of barren lands or rocks have been classified as forests in the JAXA-Forest, which were excluded in the PALSAR-2/Landsat forest. However, over the regions with dense tree cover, there are more omission errors in the JAXA-Forest map, which were identified in the PALSAR-2/Landsat forest (Fig. 10).

We further compared the five studied satellite-based forest data products in terms of their forest definitions of canopy (tree) height and canopy coverage. The frequency distributions of the forest pixels with CH and CC were extracted from different forest products using ICESat-1 observations (Fig. 11). The comparison result showed that the proportion of forest pixels with CH larger than 5-m and CC larger than 10% was 85% for NLCD-Forest in 2016, ~82% for the PALSAR-2/Landsat forest maps, 81% for the JAXA-Forest maps, 80% for the GFW-Forest in 2010 (79.98%), and 77% for Landsat VCF-Forest in 2015.

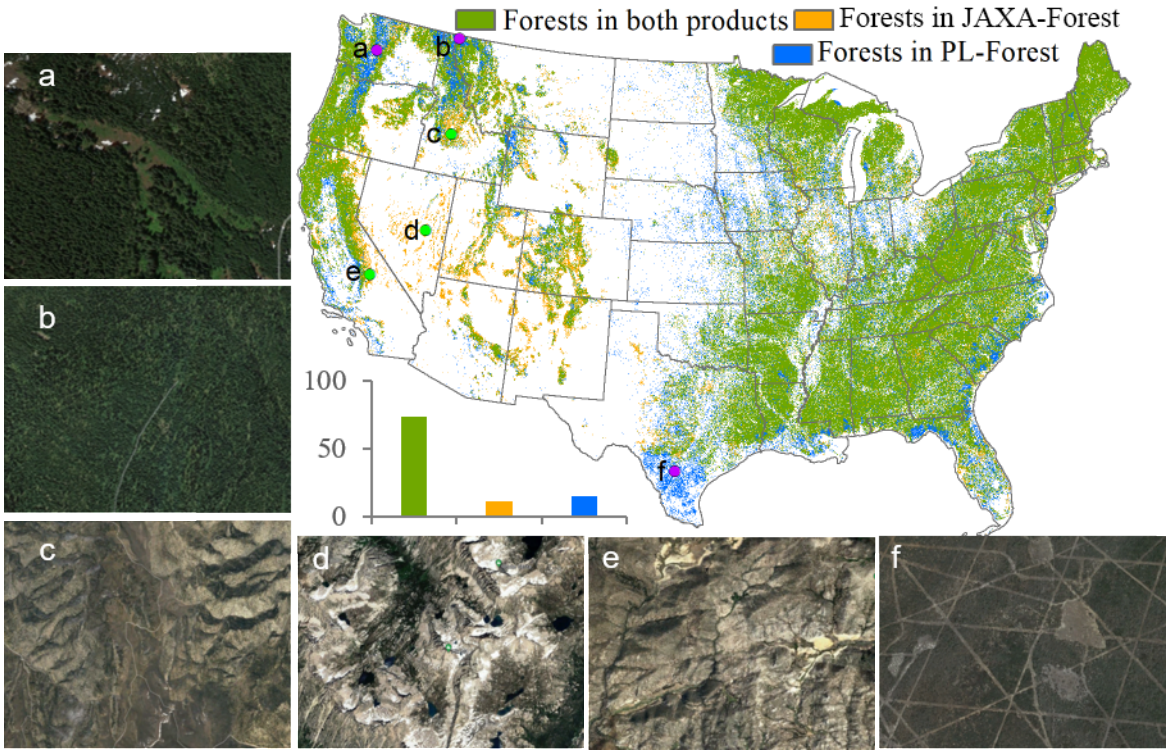

Figure 10: A comparison between the PALSAR-2/Landsat based forest (PL-Forest) map in 2016 and the Japan Aerospace Exploration Agency (JAXA) forest map in 2016 at the pixel scale. Six random areas denoted as a to f were selected from the disagreement regions, which were used to show the zoom-in landscapes from the Google Earth high-resolution images. The images were acquired from Google Earth Pro (© Google Earth Pro 2020)

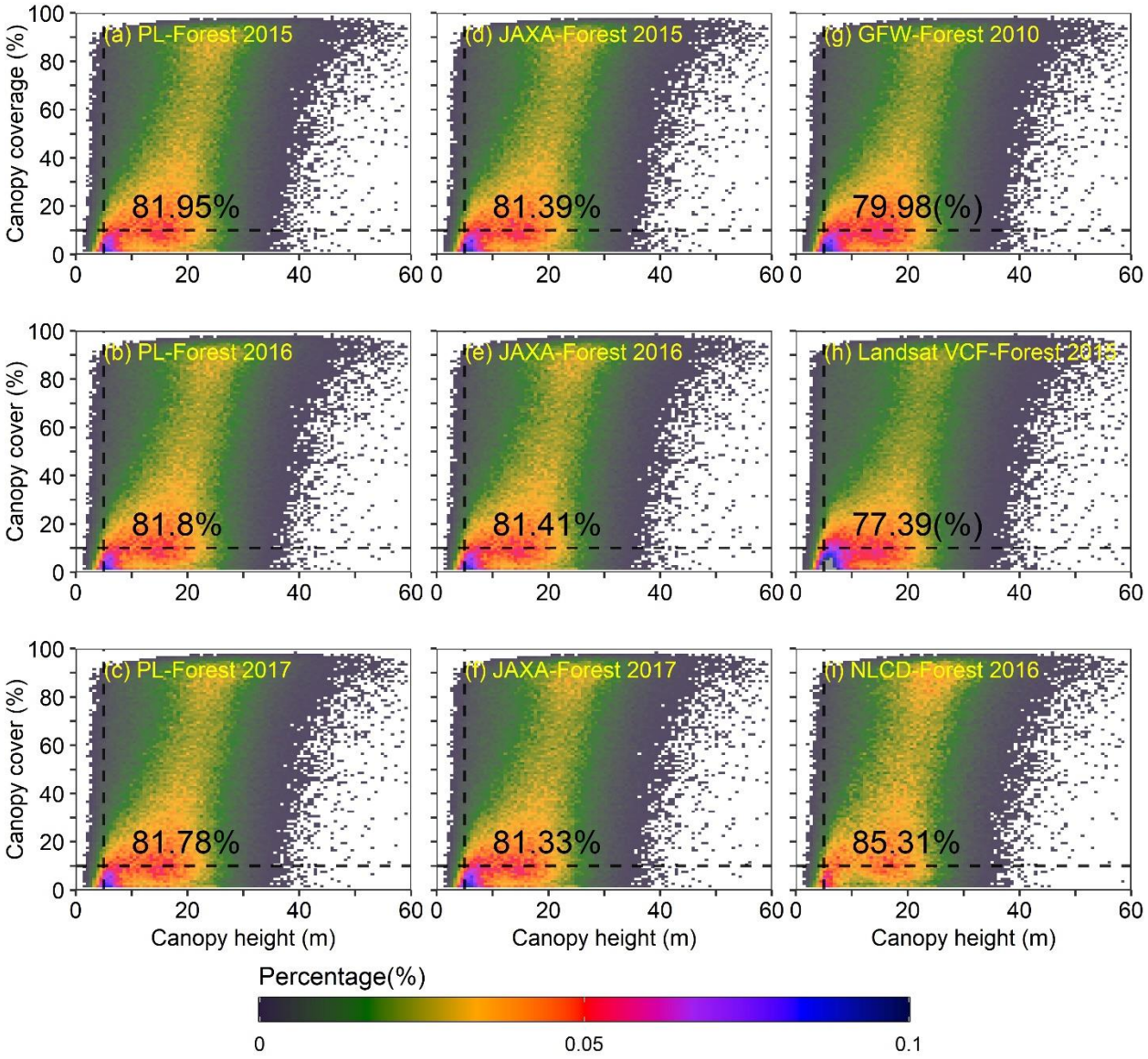

Figure 11: The frequency distributions of the forest pixels with tree canopy height (CH) and canopy cover (CC) features. The forest pixels were from the five satellite-based forest products, respectively. The CH and CC data were extracted from the ICESat-1 observations. PL-Forest is PALSAR-2/Landsat-based forest maps generated in this study. JAXA-Forest is the Japan Aerospace Exploration Agency (JAXA) forest map from 2015 to 2017. GFW-Forest 2010 is the forest map 2010 from the Global Forest Watch (GFW) program of the World Resources Institute. Landsat VCF-Forest 2015 is the Landsat-based forest cover fraction (Landsat VCF) product 2015 from the Global Land Cover Facility Data Center at the University of Maryland. The NLCD-Forest 2016 refers to the forest map from the National Land Cover Database (NLCD) in 2016 provided by the United States Geological Survey.

3.3 A comparison of forest area estimates from six forest datasets at the state and CONUS scales

The forest areas were estimated at the state and the CONUS scales from the six forest datasets, including five satellite-based forest maps in 2010-2017 and FIA statistic data in 2017 (Fig. 12). At the state scale, the PALSAR-2/Landsat forest maps have good linear relationships with other satellite-based datasets for each year during 2015 to 2017, with the slope ranging from 0.65 to 1.15, R^2 within 0.87 to 0.96 (Fig. 12a, b, c). In terms of forest area estimates

at the state scale, the PL-Forest and JAXA-Forest maps showed higher agreements with the FIA-Forest dataset than do GFW-Forest 2010, Landsat VCF-Forest 2015, and NLCD-Forest 2016 (Fig. 12d). The forest area estimates from the Landsat VCF-Forest 2015 was higher than the FIA-Forest area estimates (slope of 1.19), while the forest area estimates from the GFW-Forest 2010 and NLCD-Forest 2016 were lower than the FIA-Forest area estimates (slopes of 0.89 and 0.71) (Fig. 12d). The forest area estimates from the PL-Forest and JAXA-Forest maps were very close to the numbers from the FIA (a slope of 0.98).

At the CONUS scale, the forest area estimates from the PALSAR-2/Landsat forest maps for the years of 2015 to 2017 were 2.73×10^6 km^2, 2.79×10^6 km^2, and 2.66×10^6 km^2, respectively, which were similar to the areas of JAXA-Forest maps of 2.79×10^6 km^2, 2.68×10^6 km^2 and 2.62×10^6 km^2 (Fig. 12e). The FIA-Forest dataset reported the forest area of 2.57×10^6 km^2 in 2017, which was very close to the value of 2.66×10^6 km^2 from the PL-Forest map in 2017, a difference of 3.5%.

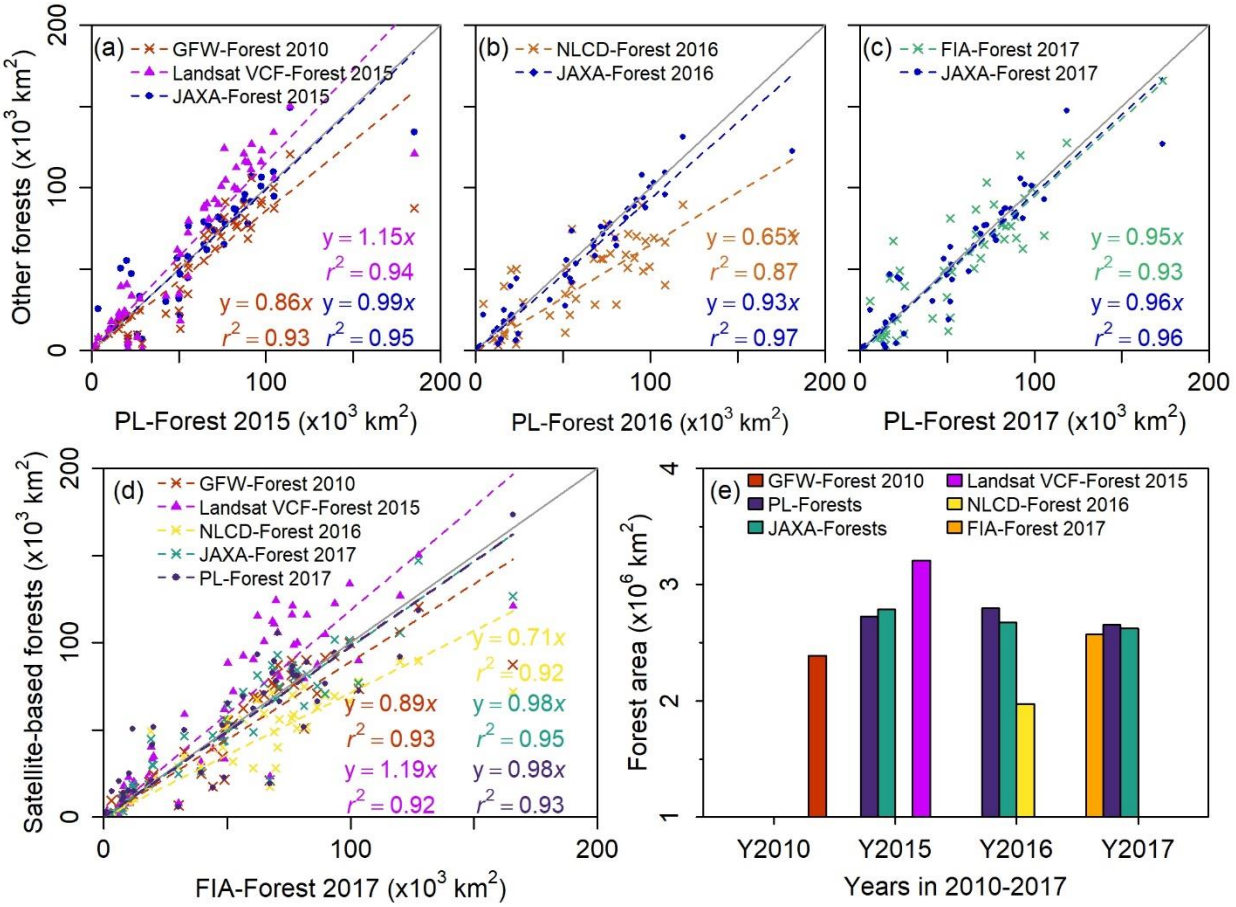

Figure 12: The comparisons of forest area estimates between satellite-based forest products and the FIA statistics at the state and national scales. PL-Forest is the PALSAR-2/Landsat-based forest map generated in this study. JAXA-Forest is

the Japan Aerospace Exploration Agency (JAXA) forest map from 2015 to 2017. GFW-Forest 2010 is the forest map in 2010 from the Global Forest Watch (GFW) program of the World Resources Institute. Landsat VCF-Forest 2015 is the Landsat-based forest cover fraction (Landsat VCF) product in 2015 from the Global Land Cover Facility Data Center at the University of Maryland. The NLCD-Forest 2016 refers to the forest map from the National Land Cover Database (NLCD) in 2016 provided by the United States Geological Survey. FIA-Forest 2017 presents the forest cover datasets from the Forest Inventory and Analysis (FIA) program in 2017.

4 Discussion

4.1 Improved annual forest maps at high spatial resolution

To improve the accuracy of forest cover maps, several efforts have examined the likely factors causing the uncertainties of the resultant products (Sexton et al., 2016; Sexton et al., 2013a; Tchuenté et al., 2011; Qin et al., 2016b). These factors include (1) the diverse forest-cover definitions, (2) input image datasets, (3) training samples, and (4) algorithms (Qin et al., 2021; Tchuenté et al., 2011). For example, the forest definitions use different criteria for tree coverage (from 10% to 60%) and tree height (from 2-m to 5-m), as well as the parcel size (Qin et al., 2016b; Sexton et al., 2016). To reduce the uncertainty of forest maps from the perspective of forest definition, a solution was proposed by Sexton et al. (2016) to focus on the measurable ecological characteristics of tree cover, canopy height, biomass, and composition of vegetation. This study provided a comprehensive assessment by intercomparison with the widely used forest products using the FAO forest definition and the Lidar-based forest structural data (CC, CH) as references. The comparison between forest datasets suggested the PL-Forest had a slightly higher percentage of pixels than JAXA-Forest, GFW-Forest 2010, and Landsat VCF-Forest 2015 in line with the FAO's forest criteria of tree height larger than 5-m and/or canopy cover larger than 10%. In this criterion, the NLCD-Forest 2016 had the highest pixel proportion, but this dataset used the tree canopy cover larger than 20% as the forest threshold and resulted in the lowest forest area estimate (Fig. 12e). This comparison results based on the PALSAR-2/Landsat forests agree well with our recent study on the forest mapping in Australia, which demonstrated that PALSAR/MODIS forest maps had more forest pixels satisfied with the FAO's forest definition than the GFW-Forest and JAXA-Forest maps (Qin et al., 2021).

Forest cover products have been generated based on the optical images (e.g., MODIS, Landsat), microwave images (e.g. PALSAR, PALSAR-2), or the integration of microwave and optical images (e.g. PALSAR/MODIS, PALSAR/Landsat). On the forest area estimates, under a consistent tree canopy cover definition (10%), the PALSAR-2/Landsat products had close results to the PALSAR-2-based forest maps for the years of 2015 to 2017 at both state and national scales (Fig. 12). The forest area estimates in 2017 from the PL-Forest dataset was very close to the result

from the FIA-Forest dataset, which indicates that the PL-Forest dataset is more accurate than the forest area estimates from the other optical satellite-based forest products (Fig. 12e). One of the reasons for the improved accuracy could be attributed to the utilization of L-band PALSAR-2 images that (1) are less affected by atmospheric conditions, clouds, and cloud shadows than optical data, and (2) have stronger penetration capability into forest canopy with more sensitivity to forest structure (Shimada et al., 2014). Our previous studies also showed the similar forest area estimates from the PALSAR/MODIS or PALSAR/Landsat forest products and the JAXA forest maps in several regions like monsoon Asia (Qin et al., 2016b), and South America (Qin et al., 2017). For example, in South America, forest area estimates from the 30-m GFW-Forest 2010 dataset were higher than those from the 50-m PALSAR/MODIS forest products (Qin et al., 2017). In addition, GFW-Forst 2010 and Landsat VCF-Forest 2015 present the forest cover in the CONUS in the years of 2010 and 2015. The inconsistent time with the FIA-Forest in 2017 may contribute to some discrepancies between them that are difficult to quantify.

The results mentioned above also suggested that PL-Forests had a slightly better performance than the other four forest products, according to the potential of forest tree height and tree canopy cover monitoring, and forest area estimates. This result corroborates the previous claims for integrating microwave and optical images to improve the forest cover maps (Reiche et al., 2015; Lehmann et al., 2015; Thapa et al., 2014). These forest mapping approaches take advantage of (1) the sensitivity of microwave signals to forest structures without weather interference (Næsset et al., 2016; Qin et al., 2016b), and (2) the optical signals to reduce the ground objects with similar backscatter values as forests, such as rocky lands and buildings (Reiche et al., 2015; Lehmann et al., 2015) (Fig. 10). The integration of PALSAR and MODIS images has been demonstrated to generate improved forest maps in tropical, temperate, and boreal forests with overall accuracies above 90% (Zhang et al., 2019; Qin et al., 2017; Qin et al., 2016b). This study produced the forest maps with an overall accuracy of about 93% which corroborated the potential of combining PALSAR-2 and Landsat observations to monitor the annual dynamics of forest distribution and functional types at a high spatial resolution for national or larger scales across the temperate regions. It also suggested the potential of integrating FIA data and PL-Forst products to support the FAO's Global Forest Resources Assessment at the national scale.

However, there could be some uncertainties and limitations when applying this approach. Firstly, although the thresholds of PALSAR-2 signatures for extracting forests were trained by numerous samples, they could be impacted by forest composition and structures (Chen et al., 2018). Thus, a careful study of the thresholds by samples of specific

areas could provide more information that affects the accuracy and uncertainty of the forest maps when applying the algorithms to other regions. In addition, due to the PALSAR data are not available during 2011-2014, we cannot apply this PALSAR/optical data approach in these four years. PALSAR data are available for 2007-2010, thus a combination of PALSAR (2007-2010), PALSAR-2 (2015 to present), and optical images would develop forest maps to monitor forest changes since 2007 (Zhang et al., 2019).

4.2 Evergreen forest mapping algorithms

Evergreen forests show different functional traits from deciduous forests, such as water use efficiency (Soh et al., 2019), and high ecosystem stability in carbon sink under extreme climates (Huang and Xia, 2019). Driven by climate change and diverse human activities, the expansion of evergreen forests has been reported in many regions all over the world (Twidwell et al., 2016; Saintilan and Rogers, 2015). Various mapping algorithms have been developed to identify evergreen and non-evergreen forests, which could provide accurate information on evergreen forests for science and policy users (Qin et al., 2016b). These evergreen forest mapping algorithms can be grouped as (1) NDVI-based and (2) LSWI-based algorithms. Evergreen plants keep green leaves in the winter season or dry season and yield high NDVI values in contrast to senescent plants. Following this phenological feature, evergreen plants and forests have been successfully separated from non-evergreen plants based on the seasonal dynamics of NDVI, for example using mean or median NDVI values of the winter season (Qin et al., 2016b; Soudani et al., 2012). Evergreen forests have LSWI values of above zero throughout the year, which has been used to map evergreen forests for tropical regions (Qin et al., 2016b; Grogan et al., 2016). In this study, the LSWI-based algorithm was used to identify the evergreen forests in CONUS and the results have reasonable consistency with the NLCD-2016 evergreen forest product (Fig. 9). It demonstrated the potential of the LSWI-based algorithm for the evergreen forest identification over the temperate regions based on Landsat datasets.

The moderate discrepancy in the evergreen forest products between the PL-Forest maps and the NLCD-2016 dataset could be attributed in part to the differences in the algorithms and image data. The NLCD products were generated using the decision tree algorithm and multi-temporal images (Jin et al., 2019). The classification algorithm is based on the spatial statistics of images (image-based spatial statistics) and training samples to generate classification rules. Therefore, the resultant forest maps are affected by the quantity and quality of the training samples. In comparison, we used the LSWI-based algorithm and time series images in a year to identify forests for individual pixels, which used pixel-based time series statistics. Our method used all the images in a year, which is more than the

multi-temporal images used in the image-based spatial statistic approach. A challenge for the LSWI-base algorithm is to acquire a sufficient number of good quality observations throughout the year, particularly, during the winter season. As Landsat acquires images at a 16-day revisit cycle, the missing data issue could cause some uncertainties in the PALSAR-2/Landsat evergreen forest maps. However, this data issue could be improved by combining multi-source remote sensing images like Sentinle-2, Landsat-8, and Landsat-9 in the future. To improve the evergreen forest mapping, the development of a hybrid approach of both LSWI- and NDVI-based algorithms is another promising way, which will be examined in our following works for discrimination of evergreen and deciduous trees, shrubs, and grasses.

Data availability

The data are available at https://doi.org/10.6084/m9.figshare.21270261(Wang, 2024).

Conclusions

This study integrated microwave (PALSAR-2) and optical (Landsat) images and produced annual forest maps in 2015-2017 for the CONUS at 30-m spatial resolution with an improved accuracy. Furthermore, we generated the annual 30-m evergreen forest maps in the CONUS, which can be used to investigate how climate change and human activities affect these forest types in the CONUS. In addition, following the FAO's forest definition, we compared the widely-used Landsat-based, PALSAR-2-based, and PALSAR-2/Landsat-based forest cover products on the characterization of forest structure metrics (CC and CH) by using the ICESat LiDAR tree structure datasets. We also compared the satellite-based forest cover products and the FIA statistical data on the forest area estimates. The comprehensive intercomparison with a wide range of products provides insights to apply appropriate products for relevant research and management activities.

Competing interests

The authors declare that they have no known competing financial interests or personal relationships that could have appeared to influence the work reported in this paper.

Author contribution

Xiangming Xiao and Jie Wang designed the experiments and Jie Wang carried them out. Jie Wang, Yuanwei Qin, Jinwei Dong developed the model code. Jie Wang prepared the manuscript with contributions from all co-authors.

Acknowledgements

The authors greatly appreciated the free access to the PALSAR-2, Landsat datasets provided by USGS and Google Earth Engine cloud computing platform, the public forest datasets of GFW in 2010 from the GLAD, the Landsat VCF in 2015 from the LCLUC, JAXA forest and non-forest maps in 2015-2017, the NLCD land cover map in 2016 from USGS, the forest statistical data for year 2017 from the USDA, and the free access to the validation samples provided by the Tsinghua University. We also thank the editor and reviewers for the insightful comments and suggestions.

Financial support

This study is funded by the Key Research and Development Program of Ningxia Province, China (2022BEG03050), the National Natural Science Foundation of China (42101355), the National Science Foundation (IIA-1920946, IIA-1946093), and USDA National Institute of Food and Agriculture (2016-68002-24967).

References

Achard, F., Eva, H., and Mayaux, P.: Tropical forest mapping from coarse spatial resolution satellite data: production and accuracy assessment issues, Int. J. Remote Sens., 22, 2741-2762, 2001.

Betts, M. G., Wolf, C., Ripple, W. J., Phalan, B., Millers, K. A., Duarte, A., Butchart, S. H., and Levi, T.: Global forest loss disproportionately erodes biodiversity in intact landscapes, Nature, 547, 441-444, 2017.

Bonan, G. B.: Forests and climate change: Forcings, feedbacks, and the climate benefits of forests, Science, 320, 1444-1449, 2008.

Burrill, E. A., DiTommaso, A. M., Turner, J. A., Pugh, S. A., Menlove, J., Christiansen, G., Perry, C. J., and Conkling, B. L.: The Forest Inventory and Analysis Database: database description and user guide version 9.0.1 for Phase 2, U.S. Department of Agriculture, Forest Service, 1026 p, 2021.

Chen, B. Q., Xiao, X. M., Ye, H. C., Ma, J., Doughty, R., Li, X. P., Zhao, B., Wu, Z. X., Sun, R., Dong, J. W., Qin, Y. W., and Xie, G. S.: Mapping Forest and Their Spatial-Temporal Changes From 2007 to 2015 in Tropical Hainan Island by Integrating ALOS/ALOS-2 L-Band SAR and Landsat Optical Images, Ieee Journal of Selected Topics in Applied Earth Observations and Remote Sensing, 11, 852-867, 10.1109/Jstars.2018.2795595, 2018.

Chen, J., Chen, J., Liao, A., Cao, X., Chen, L., Chen, X., He, C., Han, G., Peng, S., and Lu, M.: Global land cover mapping at 30 m resolution: A POK-based operational approach, Isprs J Photogramm, 103, 7-27, 2015.

Cooperation, C. f. E.: Ecological regions of North America: toward a common perspective, The Commission1997.

D'Almeida, C., Vörösmarty, C. J., Hurtt, G. C., Marengo, J. A., Dingman, S. L., and Keim, B. D.: The effects of deforestation on the hydrological cycle in Amazonia: a review on scale and resolution, International Journal of Climatology: A Journal of the Royal Meteorological Society, 27, 633-647, 2007.

Deb Burman, P. K., Launiainen, S., Mukherjee, S., Chakraborty, S., Gogoi, N., Murkute, C., Lohani, P., Sarma, D., and Kumar, K.: Ecosystem-atmosphere carbon and water exchanges of subtropical evergreen and deciduous forests in India, For. Ecol. Manag., 495, 119371, https://doi.org/10.1016/j.foreco.2021.119371, 2021.

DiMiceli, C., Carroll, M., Sohlberg, R., Huang, C., Hansen, M., and Townshend, J.: Annual global automated MODIS vegetation continuous fields (MOD44B) at 250 m spatial resolution for data years beginning day 65, 2000? 2010, collection 5 percent tree cover, University of Maryland, College Park, MD, USA, 2017.

Domke, G. M., Walters, B. F., Nowak, D. J., Smith, J., Nichols, M. C., Ogle, S. M., Coulston, J., and Wirth, T. J. R. U. F. M., WI: US Department of Agriculture, Forest Service, Northern Research Station. 5 p.. Greenhouse gas emissions and removals from forest land, woodlands, and urban trees in the United States, 1990–2019, 307, 2021.

FAO: Forest Resources Assessments (FRA2010), 2012.

Foley, J. A., DeFries, R., Asner, G. P., Barford, C., Bonan, G., Carpenter, S. R., Chapin, F. S., Coe, M. T., Daily, G. C., Gibbs, H. K., Helkowski, J. H., Holloway, T., Howard, E. A., Kucharik, C. J., Monfreda, C., Patz, J. A., Prentice, I. C., Ramankutty, N., and Snyder, P. K.: Global consequences of land use, Science, 309, 570-574, 2005.

Friedl, M. A., Sulla-Menashe, D., Tan, B., Schneider, A., Ramankutty, N., Sibley, A., and Huang, X. M.: MODIS Collection 5 global land cover: Algorithm refinements and characterization of new datasets, Remote Sens. Environ., 114, 168-182, 2010.

Gong, P., Wang, J., Yu, L., Zhao, Y. C., Zhao, Y. Y., Liang, L., Niu, Z. G., Huang, X. M., Fu, H. H., Liu, S., Li, C. C., Li, X. Y., Fu, W., Liu, C. X., Xu, Y., Wang, X. Y., Cheng, Q., Hu, L. Y., Yao, W. B., Zhang, H., Zhu, P., Zhao, Z. Y., Zhang, H. Y., Zheng, Y. M., Ji, L. Y., Zhang, Y. W., Chen, H., Yan, A., Guo, J. H., Yu, L., Wang, L., Liu, X. J., Shi, T. T., Zhu, M. H., Chen, Y. L., Yang, G. W., Tang, P., Xu, B., Giri, C., Clinton, N., Zhu, Z. L., Chen, J., and Chen, J.: Finer resolution observation and monitoring of global land cover: first mapping results with Landsat TM and ETM+ data, Int. J. Remote Sens., 34, 2607-2654, 2013.

Grogan, K., Pflugmacher, D., Hostert, P., Verbesselt, J., and Fensholt, R.: Mapping Clearances in Tropical Dry Forests Using Breakpoints, Trend, and Seasonal Components from MODIS Time Series: Does Forest Type Matter?, Remote Sens-Basel, 8, 10.3390/rs8080657, 2016.

Hansen, M., Potapov, P., Moore, R., Hancher, M., Turubanova, S., Tyukavina, A., Thau, D., Stehman, S., Goetz, S., and Loveland, T.: High-resolution global maps of 21st-century forest cover change, Science, 342, 850-853, 2013a.

Hansen, M. C. and DeFries, R. S.: Detecting long-term global forest change using continuous fields of tree-cover maps from 8-km advanced very high resolution radiometer (AVHRR) data for the years 1982-99, Ecosystems, 7, 695-716, 10.1007/s10021-004-0243-3, 2004.

Hansen, M. C., DeFries, R. S., Townshend, J. R. G., Carroll, M., Dimiceli, C., and Sohlberg, R. A.: Global Percent Tree Cover at a Spatial Resolution of 500 Meters: First Results of the MODIS Vegetation Continuous Fields Algorithm, Earth Interact, 7, 2003.

Hansen, M. C., Potapov, P. V., Moore, R., Hancher, M., Turubanova, S., Tyukavina, A., Thau, D., Stehman, S., Goetz, S., and Loveland, T.: High-resolution global maps of 21st-century forest cover change, Science, 342, 850-853, 2013b.

Harris, N. L., Brown, S., Hagen, S. C., Saatchi, S. S., Petrova, S., Salas, W., Hansen, M. C., Potapov, P. V., and Lotsch, A.: Baseline map of carbon emissions from deforestation in tropical regions, Science, 336, 1573-1576, 2012.

Homer, C., Dewitz, J., Jin, S., Xian, G., Costello, C., Danielson, P., Gass, L., Funk, M., Wickham, J., Stehman, S., Auch, R., and Riitters, K.: Conterminous United States land cover change patterns 2001–2016 from the 2016 National Land Cover Database, Isprs J Photogramm, 162, 184-199, https://doi.org/10.1016/j.isprsjprs.2020.02.019, 2020.

Hoover, C. M., Bush, R., Palmer, M., and Treasure, E.: Using Forest Inventory and Analysis Data to Support National Forest Management: Regional Case Studies, Journal of Forestry, 118, 313-323, 10.1093/jofore/fvz073, 2020.

Huang, K. and Xia, J.: High ecosystem stability of evergreen broadleaf forests under severe droughts, Global Change Biology, 25, 3494-3503, https://doi.org/10.1111/gcb.14748, 2019.

Jin, S., Yang, L., Danielson, P., Homer, C., Fry, J., and Xian, G.: A comprehensive change detection method for updating the National Land Cover Database to circa 2011, Remote Sens. Environ., 132, 159-175, 2013a.

Jin, S., Homer, C., Yang, L., Danielson, P., Dewitz, J., Li, C., Zhu, Z., Xian, G., and Howard, D.: Overall Methodology Design for the United States National Land Cover Database 2016 Products, Remote Sens-Basel, 11, 2971, 2019.

Jin, S. M., Yang, L. M., Danielson, P., Homer, C., Fry, J., and Xian, G.: A comprehensive change detection method for updating the National Land Cover Database to circa 2011, Remote Sens. Environ., 132, 159-175, DOI 10.1016/j.rse.2013.01.012, 2013b.

Knott, J. A., Desprez, J. M., Oswalt, C. M., and Fei, S. L.: Shifts in forest composition in the eastern United States, For. Ecol. Manag., 433, 176-183, 10.1016/j.foreco.2018.10.061, 2019.

Kushwaha, S. P. S.: Forest-Type Mapping and Change Detection from Satellite Imagery, Isprs J Photogramm, 45, 175-181, 1990.

Laurin, G. V., Puletti, N., Hawthorne, W., Liesenberg, V., Corona, P., Papale, D., Chen, Q., and Valentini, R.: Discrimination of tropical forest types, dominant species, and mapping of functional guilds by hyperspectral and simulated multispectral Sentinel-2 data, Remote Sens. Environ., 176, 163-176, 10.1016/j.rse.2016.01.017, 2016.

Lehmann, E. A., Caccetta, P., Lowell, K., Mitchell, A., Zhou, Z.-S., Held, A., Milne, T., and Tapley, I.: SAR and optical remote sensing: Assessment of complementarity and interoperability in the context of a large-scale operational forest monitoring system, Remote Sens. Environ., 156, 335-348, 2015.

Mekonnen, Z. A., Riley, W. J., Randerson, J. T., Grant, R. F., and Rogers, B. M.: Expansion of high-latitude deciduous forests driven by interactions between climate warming and fire, Nature Plants, 5, 952-958, 10.1038/s41477-019-0495-8, 2019.

Næsset, E., Ørka, H. O., Solberg, S., Bollandsås, O. M., Hansen, E. H., Mauya, E., Zahabu, E., Malimbwi, R., Chamuya, N., Olsson, H., and Gobakken, T.: Mapping and estimating forest area and aboveground biomass in miombo woodlands in Tanzania using data from airborne laser scanning, TanDEM-X, RapidEye, and global forest maps: A comparison of estimated precision, Remote Sens. Environ., 175, 282-300, http://dx.doi.org/10.1016/j.rse.2016.01.006, 2016.

Oswalt;, S. N., Smith;, W. B., Miles;, P. D., and Pugh, S. A.: Assessment of the influence of disturbance, management activities, and environmental factors on carbon stocks of U.S. national forests, Gen. Tech. Rep. WO-97. Washington, DC: U.S. Department of Agriculture, Forest Service, Washington Office., 2019.

Peng, S. S., Piao, S. L., Zeng, Z. Z., Ciais, P., Zhou, L. M., Li, L. Z. X., Myneni, R. B., Yin, Y., and Zeng, H.: Afforestation in China cools local land surface temperature, Proc. Natl. Acad. Sci. U. S. A., 111, 2915-2919, 2014.

Prabakaran, C., Singh, C., Panigrahy, S., and Parihar, J. J. C. S.: Retrieval of forest phenological parameters from remote sensing-based NDVI time-series data, 795-802, 2013.

Qin, Y., Xiao, X., Tang, H., Dubayah, R., Doughty, R., Liu, D., Liu, F., Shimabukuro, Y., Arai, E., and Wang, X. J. E. S. S. D.: Annual maps of forest cover in the Brazilian Amazon from analyses of PALSAR and MODIS images, Earth Syst Sci Data, 16, 321-336, 2024.

Qin, Y., Xiao, X., Wigneron, J.-P., Ciais, P., Canadell, J. G., Brandt, M., Li, X., Fan, L., Wu, X., and Tang, H.: Annual Maps of Forests in Australia from Analyses of Microwave and Optical Images with FAO Forest Definition, Journal of Remote Sensing, 2021, 2021.

Qin, Y., Xiao, X., Wang, J., Dong, J., Ewing, K., Hoagland, B., Hough, D., Fagin, T., Zou, Z., Geissler, G., Xian, G., and Loveland, T.: Mapping Annual Forest Cover in Sub-Humid and Semi-Arid Regions through Analysis of Landsat and PALSAR Imagery, Remote Sens-Basel, 8, 933, 2016a.

Qin, Y. W., Xiao, X. M., Dong, J. W., Zhou, Y. T., Wang, J., Doughty, R. B., Chen, Y., Zou, Z. H., and Moore, B.: Annual dynamics of forest areas in South America during 2007-2010 at 50m spatial resolution, Remote Sens. Environ., 201, 73-87, 2017.

Qin, Y. W., Xiao, X. M., Dong, J. W., Zhang, Y., Wu, X. C., Shimabukuro, Y., Arai, E., Biradar, C., Wang, J., Zou, Z. H., Liu, F., Shi, Z., Doughty, R., and Moore, B.: Improved estimates of forest cover and loss in the Brazilian Amazon in 2000-2017, Nature Sustainability, 2, 764-772, 10.1038/s41893-019-0336-9, 2019.

Qin, Y. W., Xiao, X. M., Dong, J. W., Zhang, G. L., Roy, P. S., Joshi, P. K., Gilani, H., Murthy, M. S. R., Jin, C., Wang, J., Zhang, Y., Chen, B. Q., Menarguez, M. A., Biradar, C. M., Bajgain, R., Li, X. P., Dai, S. Q., Hou, Y., Xin, F. F., and Moore, B.: Mapping forests in monsoon Asia with ALOS PALSAR 50-m mosaic images and MODIS imagery in 2010, Sci Rep-Uk, 6, ARTN 20880
10.1038/srep20880, 2016b.

Reiche, J., Verbesselt, J., Hoekman, D., and Herold, M.: Fusing Landsat and SAR time series to detect deforestation in the tropics, Remote Sens. Environ., 156, 276-293, 2015.

Reiche, J., Hamunyela, E., Verbesselt, J., Hoekman, D., and Herold, M.: Improving near-real time deforestation monitoring in tropical dry forests by combining dense Sentinel-1 time series with Landsat and ALOS-2 PALSAR-2, Remote Sens. Environ., 204, 147-161, 2018.

Ruefenacht, B., Finco, M., Nelson, M., Czaplewski, R., Helmer, E., Blackard, J., Holden, G., Lister, A., Salajanu, D., and Weyermann, D.: Conterminous US and Alaska forest type mapping using forest inventory and analysis data, Photogramm Eng Rem S, 74, 1379-1388, 2008.

Saintilan, N. and Rogers, K.: Woody plant encroachment of grasslands: a comparison of terrestrial and wetland settings, New Phytol., 205, 1062-1070, Doi 10.1111/Nph.13147, 2015.

Selkowitz, D. J. and Stehman, S. V.: Thematic accuracy of the National Land Cover Database (NLCD) 2001 land cover for Alaska, Remote Sens. Environ., 115, 1401-1407, https://doi.org/10.1016/j.rse.2011.01.020, 2011.

Seto, K. C., Guneralp, B., and Hutyra, L. R.: Global forecasts of urban expansion to 2030 and direct impacts on biodiversity and carbon pools, Proc. Natl. Acad. Sci. U. S. A., 109, 16083-16088, 10.1073/pnas.1211658109, 2012.

Sexton, J. O., Noojipady, P., Song, X.-P., Feng, M., Song, D.-X., Kim, D.-H., Anand, A., Huang, C., Channan, S., and Pimm, S. L.: Conservation policy and the measurement of forests, Nat Clim Change, 6, 192-196, 2016.

Sexton, J. O., Noojipady, P., Song, X.-P., Feng, M., Song, D.-X., Kim, D.-H., Anand, A., Huang, C., Channan, S., Pimm, S. L., and Townshend, J. R.: Conservation policy and the measurement of forests, Nature Climate Change, 6, 192-196, 10.1038/nclimate2816, 2015.

Sexton, J. O., Song, X.-P., Feng, M., Noojipady, P., Anand, A., Huang, C., Kim, D.-H., Collins, K. M., Channan, S., DiMiceli, C., and Townshend, J. R.: Global, 30-m resolution continuous fields of tree cover: Landsat-based rescaling of MODIS vegetation continuous fields with lidar-based estimates of error, International Journal of Digital Earth, 6, 427-448, 10.1080/17538947.2013.786146, 2013a.

Sexton, J. O., Song, X. P., Feng, M., Noojipady, P., Anand, A., Huang, C. Q., Kim, D. H., Collins, K. M., Channan, S., DiMiceli, C., and Townshend, J. R.: Global, 30-m resolution continuous fields of tree cover: Landsat-based rescaling of MODIS vegetation continuous fields with lidar-based estimates of error, Int J Digit Earth, 6, 427-448, 10.1080/17538947.2013.786146, 2013b.

Shimada, M., Isoguchi, O., Tadono, T., and Isono, K.: PALSAR Radiometric and Geometric Calibration, Ieee Transactions on Geoscience and Remote Sensing, 47, 3915-3932, 2009.

Shimada, M., Itoh, T., Motooka, T., Watanabe, M., Shiraishi, T., Thapa, R., and Lucas, R.: New global forest/non-forest maps from ALOS PALSAR data (2007-2010), Remote Sens. Environ., 155, 13-31, 2014.

Smith, W. B., Lara, R. A. C., Caballero, C. E. D., Valdivia, C. I. G., Kapron, J. S., Reyes, J. C. L., Tovar, C. L. M., Miles, P. D., Oswalt, S. N., and Salgado, M. R.: The North American Forest Database: going beyond national-level forest resource assessment statistics, Environ. Monit. Assess., 190, 350, 2018.

Soh, W. K., Yiotis, C., Murray, M., Parnell, A., Wright, I. J., Spicer, R. A., Lawson, T., Caballero, R., and McElwain, J. C.: Rising CO2 drives divergence in water use efficiency of evergreen and deciduous plants, Sci Adv, 5, eaax7906, 2019.

Soudani, K., Hmimina, G., Delpierre, N., Pontailler, J. Y., Aubinet, M., Bonal, D., Caquet, B., de Grandcourt, A., Burban, B., Flechard, C., Guyon, D., Granier, A., Gross, P., Heinesh, B., Longdoz, B., Loustau, D., Moureaux, C., Ourcival, J. M., Rambal, S., Saint André, L., and Dufrêne, E.: Ground-based Network of NDVI measurements for tracking temporal dynamics of canopy structure and vegetation phenology in different biomes, Remote Sens. Environ., 123, 234-245, https://doi.org/10.1016/j.rse.2012.03.012, 2012.

Souza, C., Firestone, L., Silva, L. M., and Roberts, D.: Mapping forest degradation in the Eastern Amazon from SPOT 4 through spectral mixture models, Remote Sens. Environ., 87, 494-506, 10.1016/j.rse.2002.08.002, 2003.

Stibig, H.-J. and Malingreau, J.-P.: Forest cover of insular Southeast Asia mapped from recent satellite images of coarse spatial resolution, AMBIO: A Journal of the Human Environment, 32, 469-475, 2003.

Stibig, H. J., Achard, F., and Fritz, S.: A new forest cover map of continental southeast Asia derived from SPOT-VEGETATION satellite imagery, Appl. Veg. Sci., 7, 153-162, 2004.

Tang, H., Armston, J., Hancock, S., Marselis, S., Goetz, S., and Dubayah, R.: Characterizing global forest canopy cover distribution using spaceborne lidar, Remote Sens. Environ., 231, 111262, https://doi.org/10.1016/j.rse.2019.111262, 2019.

Tchuenté, A. T. K., Roujean, J.-L., and De Jong, S. M.: Comparison and relative quality assessment of the GLC2000, GLOBCOVER, MODIS and ECOCLIMAP land cover data sets at the African continental scale, Int J Appl Earth Obs, 13, 207-219, 2011.

Thapa, R. B., Itoh, T., Shimada, M., Watanabe, M., Takeshi, M., and Shiraishi, T.: Evaluation of ALOS PALSAR sensitivity for characterizing natural forest cover in wider tropical areas, Remote Sens. Environ., 155, 32-41, 2014.

Tran, T. V., de Beurs, K. M., and Julian, J. P.: Monitoring forest disturbances in Southeast Oklahoma using Landsat and MODIS images, Int J Appl Earth Obs, 44, 42-52, https://doi.org/10.1016/j.jag.2015.07.001, 2016.

Twidwell, D., West, A. S., Hiatt, W. B., Ramirez, A. L., Winter, J. T., Engle, D. M., Fuhlendorf, S. D., and Carlson, J.: Plant invasions or fire policy: which has altered fire behavior more in tallgrass prairie?, Ecosystems, 19, 356-368, 2016.

Vermote, E., Justice, C., Claverie, M., and Franch, B.: Preliminary analysis of the performance of the Landsat 8/OLI land surface reflectance product, Remote Sens. Environ., 185, 46-56, 10.1016/j.rse.2016.04.008, 2016.

Wang, J.: 30m PALSAR-2/Landsat-based Forest and Evergreen Forest maps in CONUS from 2015 to 2017, 10.6084/m9.figshare.21270261.v2, 2024.

Zhang, Y., Ling, F., Foody, G. M., Ge, Y., Boyd, D. S., Li, X., Du, Y., and Atkinson, P. M.: Mapping annual forest cover by fusing PALSAR/PALSAR-2 and MODIS NDVI during 2007–2016, Remote Sens. Environ., 224, 74-91, https://doi.org/10.1016/j.rse.2019.01.038, 2019.